JGR Solid Earth

RESEARCH ARTICLE
10.1029/2019JB017914

New Evidence of 'Anomalous' Vertical Movements along the Hinterland of the Atlantic NW African Margin

M. Gouiza[1], G. Bertotti[2], R. Charton[2], K. Haimoudane[3], I. Dunkl[4], and A. A. Anczkiewicz[5]

[1]Basin Structure Group (BSG), School of Earth and Environment, University of Leeds, Leeds, UK, [2]Department of Geoscience and Engineering, Delft University of Technology, Delft, The Netherlands, [3]The Mauritanian Office for Geological Exploration (OMRG), Nouakchott, Mauritania, [4]Geoscience Centre, Goettingen University, Göttingen, Germany, [5]Institute of Geological Sciences, Polish Academy of sciences, Research Centre in Kraków, Kraków, Poland

Key Points:
- New low-temperature thermochronology data reveal major anomalous thermal events in the hinterland of the Atlantic NW African margin
- Mauritanian Atlantic margin experienced two major post-Variscan cooling events, during Jurassic–Cretaceous and Neogene times
- Intraplate stresses associated with the geodynamic evolutions of the Atlantic and the African plate control post-rift vertical movements

Correspondence to:
M. Gouiza,
m.gouiza@leeds.ac.uk

Citation:
Gouiza, M., Bertotti, G., Charton, R., Haimoudane, K., Dunkl, I., & Anczkiewicz, A. A. (2019). New evidence of 'anomalous' vertical movements along the hinterland of the atlantic NW african margin. *Journal of Geophysical Research: Solid Earth*, *124*, 13,333–13,353. https://doi.org/10.1029/2019JB017914

Received 25 APR 2019
Accepted 20 NOV 2019
Accepted article online 23 NOV 2019
Published online 11 DEC 2019

Abstract Low-temperature thermochronology studies revealed major exhumation events affecting domains in the hinterland of the Central Atlantic margins, where Palaeozoic and/or Precambrian basement is exposed. Thus, domains traditionally assumed to be stable since at least the Variscan and juxtaposed to subsiding Meso-Cenozoic basins, appear to be affected by km-scale vertical movements during the Atlantic rifting and after the Early Jurassic breakup in the Central Atlantic. In this contribution, we investigate the extent and the magnitude of these motions along the NW African margin by presenting the first low-temperature thermochronology data from west Mauritania. The analysed 22 samples were collected along the Mauritanides, a N-S trending Variscan Belt separating the cratonic Taoudeni Basin in the east from the Atlantic coastal basin in the west. The obtained apatite fission track (AFT) ages range between 236 and 90 Ma, with mean track lengths between 11.22 and 12.81 μm and D_{par} comprised between 1.6 and 2.1 μm. The uncorrected (U-Th-Sm)/He (AHe) ages vary between 261 and 33 Ma. Inverse thermal modelling of the AFT and AHe data indicates that the hinterland of the Mauritanian Atlantic margin experienced (i) burial between the Permian and the Late Triassic, (ii) km-scale exhumation during Middle-Late Jurassic and Early Cretaceous, (iii) burial during the Palaeogene–early Miocene, and (iv) exhumation between mid-Miocene and present-day. We argue that these vertical movements are primarily driven by the tectonic evolution of the Atlantic rift and the subsequent geodynamic evolution of the Central Atlantic Ocean and the African plate.

1. Introduction

The history of vertical movements around the Central Atlantic has been the subject of many studies in the last decade that revealed the existence of unexpected km-scale exhumation and burial events (e.g., Charton et al., 2018; Ghorbal et al., 2008; Gouiza et al., 2017, 2018; Leprêtre et al., 2017; Lorencak et al., 2004; RodenTice & Tice, 2005; RodenTice et al., 2000; Ruiz et al., 2011; Saddiqi et al., 2009; Taylor & Fitzgerald, 2011; Teixell et al., 2009). The intriguing aspects of these findings are the timing and the magnitude of the exhumation, as 2 to 4 km of upward motions were recorded during Jurassic to Cretaceous times, which is shortly after the Early Jurassic breakup in the Central Atlantic and prior to the main Cenozoic Alpine shortening events. The exhumation affected various domains in the hinterland of the NW African margin, where Palaeozoic and/or Precambrian basement is exposed (e.g., Western Meseta, High Atlas of Marrakech, Anti-Atlas, and Reguibat Shield). Concurrently, subsidence continued in the nearby offshore and coastal Atlantic basins, documented by the accumulation of thick Jurassic to Cretaceous pile of sediments (e.g., Bertotti & Gouiza, 2012; Charton et al., 2018; Ellouz et al., 2003; Gouiza et al., 2010).

Km-scale post-rift exhumation events are recorded along many other margins in the North Atlantic (e.g., Japsen et al., 2012; Bonnin et al., 2014), South Atlantic (e.g., Cogné et al., 2011; Harman et al., 1998), and West Australia (e.g., Gallagher & Brown, 1997; Weber et al., 2005). Thus, such events appear to be a rule rather than an exception in the evolution of newly formed rifted margins. They are usually qualified as 'unexpected' or 'anomalous' because they do not fit in the classical McKenzie model of passive margins, which is widely used and predicts a prolonged passive thermal cooling/subsidence after breakup (McKenzie, 1978; Steckler & Watts, 1982; Watts, 1982). Burov and Cloetingh (1997) on the other hand used thermo-mechanical modelling to show that rift shoulder exhumation, if coupled with erosion, can persist for a long period of time after continental breakup (> 30 Myr).

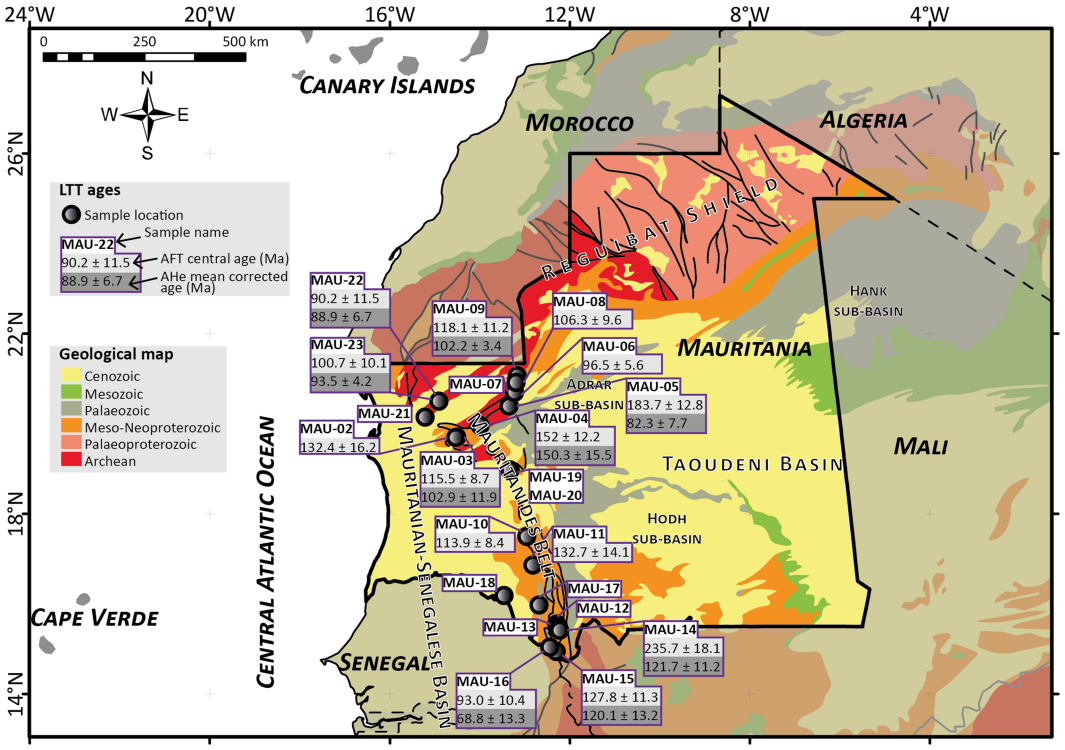

Figure 1. Simplified geological map of Mauritania and surroundings (Thiéblemont, 2016), showing the location of the low-temperature thermochronology samples and corresponding AHe corrected mean ages and/or AFT central ages.

Quantifying the timing, magnitude, and wavelength of exhumation, and associated denudation, is crucial to understand processes controlling rifted margin evolution, which should be considered in assessing hydrocarbon maturation, migration pathways and reservoirs. This study investigates the southward extent of the Mesozoic exhumation events, already documented in the northern part of the NW African margin, with new samples collected from the Reguibat Shield and along the Mauritanides fold belt in Mauritania. This is the first extensive low-temperature thermochronology dataset and associated inverse thermal modelling along the Mauritanian Atlantic margin.

2. Geological Setting

The geological map of Mauritania shows four distinct tectono-stratigraphic domains (Figure 1): (1) the Precambrian Reguibat shield in the north, (2) the Palaeozoic Toudeni Basin in the east, (3) the Mauritanides belt in the centre, and (4) the Mesozoic Atlantic coastal basin in the west (i.e., Mauritanian-Senegalese Basin). The Reguibat Shield is an elongated ENE-WSW domain, where the West African Craton (WAC) basement is exposed. It consists of granitic and metamorphic Archean rocks in the west and granitic and volcano-sedimentary Palaeoproterozoic rocks in the east (Schofield et al., 2012; Villeneuve & Cornée, 1994). The WAC sedimentary cover is preserved in the Taoudeni Basin, which is a cratonic basin filled by a thick pile of Neoproterozoic to Carboniferous sediments (up to 6 km) overlain by a major erosional unconformity, then a thin Cretaceous to Cenozoic cover (Martín-Monge et al., 2017; Villeneuve, 2005). The basin itself comprises several sub-basins but the main Palaeozoic depocentres are found in the Adrar sub-basin in the NW, the Hodh sub-basin in the centre, and the Hank sub-basin in the NE (Villeneuve, 2005). The Mauritanides fold belt extends from Morocco to Guinea Bissau, along the western boundary of the WAC. It records the Variscan tectonic events, which occurred ca. 330–270 Ma and led to the emplacement of eastward thrust sheets over the Palaeozoic sediments of the Taoudeni Basin (Purdy, 1987; Villeneuve, 2005). In Mauritania, the Mauritanides belt outcrops in a N-S corridor along the Taoudeni Basin and is largely covered by the Mesozoic to Cenozoic sediments of the Atlantic coastal basin further to the west (Figure 1). The Atlantic coastal basin extends along the onshore Mauritanian and Senegalese rifted margin (Figure 1), with thick

Mesozoic to Cenozoic sedimentary packages which gradually thin toward the east and pinch out against the Mauritanides belt (Ndiaye et al., 2016).

The geological evolution of Mauritania was affected by two major orogenies. The Pan-African Orogeny (ca. 900–500 Ma), which remnants are found in Africa, Arabian Peninsula, Brazil, North America and Europe, resulted from several collision events around the WAC during the assembly of Gondwana (e.g., Black & Liegeois, 1993; Hefferan et al., 2000). The Pan-African belts were then reactivated during the Cambrian to Late Devonian extension related to the rifting of west Gondwana (e.g., Baidder et al., 2008). The latter ended when Laurasia collided with Gondwana to form Pangea during the Variscan Orogeny (ca. 330–270 Ma), which resulted in the establishment of the N-S Mauritanides fold belt (e.g., Villeneuve, 2005). In the Triassic, continental rifting related to the opening of the Central Atlantic reactivated the Mauritanides structures (e.g., Le & Piqué, 2001; Piqué & Laville, 1996). It led to continental breakup between NW Africa and East North America by the Early-Middle Jurassic and the development of the Mauritanian Atlantic margin (Sahabi et al., 2004; Klitgord et al., 1986). The thermal effect of the Atlantic rifting extended at least to the foothills of the present-day remnants of the Mauritanides, as attested by the extent of the Mauritanian-Senegalese coastal basin (Figure 1). The latter consists of a thick pile (up to 10 km) of Late Triassic to Quaternary sediments in its western part and mostly post-Jurassic sediments in its eastern part (Brun & Lucazeau, 1988; Ndiaye et al., 2016). Thus, the thermal effect of the Atlantic rift certainly reached the Variscan basement, presently outcropping in the Mauritanides, even though the tectonic effect might have not extended that far east. The Africa-Europe convergence that initiated in the Late Cretaceous and resulted in the Atlas Orogeny in N Africa do not appear to have a major effect on the Mauritanian geology. Nevertheless, low-temperature thermochronology data from the Reguibat Shield in the north indicate a Cenozoic cooling event that some studies have linked to the far effect of the Africa-Europe convergence (Gouiza et al., 2018; Leprêtre et al., 2014).

3. Analytical Methods

Low-temperature thermochronology (LTT) techniques, like apatite fission tracks (AFT) and apatite (U-Th-Sm)/He (AHe), are widely used to constrain the near-surface thermal history, which is then interpreted in terms of vertical movements. To investigate the history of vertical movements in Mauritania, 22 samples were collected from the Precambrian crystalline basement, which sporadically outcrops 100 to 500 km east of the shoreline of the Atlantic margin (Figure 1). The large majority of the samples were taken from granitic intrusions exposed in the Reguibat Shield in the north and along the N-S trending Mauritanides belt (Table 1). The sampled non-granitic lithologies include tonalite, syenite, and metapelite, which did not yield good nor enough apatites for AFT and AHe analyses (Table 1).

3.1. Apatite Fission Tracks

The AFT method is based on the spontaneous fission of U, which results in damage trails called fission tracks. In apatite, fission tracks form with an initial etchable length of 16 ± 1 μm which anneal as function of temperature (Green et al., 1989). Tracks are completely annealed at temperatures higher than 110 °C and they are preserved with minimal annealing at temperatures lower than 60 °C (Green et al., 1989). This temperature range (110–60 °C) is called the partial annealing zone. Annealing rates are controlled primarily by temperature but also by apatite composition (i.e., F and Cl content). The etch pit diameter (D_{par}) is measured and used as proxy for the influence of chemical composition on track annealing (Donelick et al., 1999). AFT ages are obtained by measuring ^{238}U spontaneous track density relative to ^{235}U induced track density. AFT ages are combined with measurements of track lengths to quantify the thermal history of the sampled rocks (Gallagher, 2012; Ketcham et al., 2007).

AFT dating by the external detector method (Gleadow et al., 1983) was carried out at the Institute of Geological Sciences, Polish Academy of Sciences in Kraków (Poland). Apatite crystals were mounted in an epoxy resin, polished and etched in 5N HNO_3 at 20-21 °C for 20 seconds to reveal spontaneous fission tracks (Donelick et al., 1999). Samples together with age standards (Fish Canyon, Durango, and Mount Dromedary apatite) and CN5 glass dosimeters were irradiated at the TRIGA reactor (Oregon State University, USA). After the irradiation, muscovite detectors were etched for 45 minutes in 40 % HF to reveal induced fission tracks. Tracks were counted and track lengths were measured at 1250x magnification under dry objective using a NIKON Eclipse E-600 microscope, equipped with motorised stage, digitising tablet and drawing tube controlled by FTStage 4.04 software (Dumitru, 1993). Fission track ages were calculated using TrackKey

Table 1
Lithologies and coordinates (WGS84) of analysed samples

Sample Name	Lithology	Coordinates X	Coordinates Y
MAU-02	Granite-schist	-14.51	19.70
MAU-03	Granite-schist (mylonitic texture)	-14.53	19.96
MAU-04	Feldspar-Granite	-13.99	19.96
MAU-05	Feldspar-Granite	-13.35	20.39
MAU-06	Feldpar-Granite	-13.23	20.70
MAU-07	Biotite-Granite (weathered)	-13.23	20.70
MAU-08	Biotite-Granite (coarse texture)	-13.16	21.07
MAU-09	Granite-gneiss	-13.20	20.92
MAU-10	Metagranite (mylonitic texture)	-12.95	17.49
MAU-11	Metagranite (mylonitic texture)	-12.82	16.86
MAU-12	Granite (meladiorite)	-12.29	15.55
MAU-13	Muscovite-Granite (gneissic texture)	-12.27	15.48
MAU-14	Muscovite-Granite (gneissic texture)	-12.22	15.42
MAU-15	Granite-gneiss (gneissic texture)	-12.30	14.94
MAU-16	Diorite (fine texture)	-12.44	15.04
MAU-17	Metapelite (fine, pelitic quartzite)	-12.68	15.98
MAU-18	Quartzite (quartz-arenite)	-13.46	16.19
MAU-19	Syenite	-13.32	18.97
MAU-20	Tonalite	-13.33	18.97
MAU-21	Granite	-15.22	20.15
MAU-22	micro-Granite	-14.91	20.50
MAU-23	micro-Granite	-14.91	20.50

4.2g (Dunkl, 2002). The track annealing kinetics in apatite were assessed by measuring etch pit diameter (i.e., D_{par}; Burtner et al., 1994).

3.2. Apatite (U-Th-Sm)/He

The AHe method is based on radiogenic He that results from the decay of U, Th, and Sm via α-particle emission. In apatite, (U-Th-Sm)/He closure temperature depends on the crystal size and the amount of radiation damage due to α-particle recoil (Brown et al., 2013; Flowers, 2009; Gautheron et al., 2013; Reiners & Farley, 2001). Thus the partial retention zone, which is the temperature range defined by He total retention and He complete diffusive loss, can vary between 40 and 120 °C (Gautheron et al., 2013; Shuster et al., 2006).

AHe dating was carried out at the GÖochrom Laboratory of the University of Göttingen (Germany). Apatite were hand-picked under a stereo-polarizing microscope and the appropriated crystals were selected under 200x magnification according to the selection criteria of Farley (2002). The width and length of each selected crystal were measured to determine the α-ejection correction factors (Farley et al., 1996). After single apatite crystals were loaded into pre-cleaned Pt tubes, helium extraction was performed by heating the encapsulated grains in vacuum using an IR laser. The extracted gas was purified by a SAES Ti-Zr getter and the He content was measured by a Hiden Hal-3F/PIC triple-filter quadrupole mass spectrometer. For measurements of the α-emitting elements (U, Th, and Sm), the crystals were dissolved and spiked with calibrated ^{233}U, ^{230}Th, and ^{149}Sm solutions. Apatites were dissolved in 2 % ultrapure HNO_3 (+ 0.05 % HF) in an ultrasonic bath. The actinide and Sm concentrations were measured by inductively coupled plasma mass spectrometry using the isotope dilution method with a Perkin Elmer Elan DRC II system equipped with an APEX micro-flow nebulizer. Uncertainty in single-grain AHe analysis is calculated by adding analytical procedure error (i.e., related to He, U, Th, and Sm measurement) and standard deviation of the reproducibility of Durango apatite standards.

Journal of Geophysical Research: Solid Earth

10.1029/2019JB017914

Table 2
Results of Apatite Fission Track Analysis

			Dosimeter tracks		Spontaneous tracks		Induced tracks									
Sample name	No. of grains	U [ppm]	ρ_d	N_d	ρ_s	N_s	ρ_i	N_i	P(χ^2) [%]	Central age [Ma]	1σ [Ma]	MTL [µm]	MTL SE [µm]	No. of tracks	MTL SD [µm]	D_{par} [µm]
MAU-02	19	7.0	1.16	3480	0.44	116	0.62	175	100.0	132.4	16.2	12.59	0.27	32	1.6	1.6
MAU-03	20	17.4	1.13	3397	0.92	316	1.56	534	100.0	115.5	8.7	12.52	0.13	98	1.3	1.8
MAU-04	20	14.4	1.17	3499	1.03	301	1.36	397	99.8	152	12.2	12.81	0.16	70	1.4	1.8
MAU-05	20	24.3	1.13	3406	2.10	468	2.23	496	54.6	183.7	12.8	12.10	0.12	100	1.2	1.9
MAU-06	20	46.7	1.17	3527	2.08	536	4.36	1127	89.8	96.5	5.6	11.42	0.13	72	1.1	1.8
MAU-08	20	15.6	1.15	3462	0.81	205	1.52	384	90.0	106.3	9.6	12.28	0.12	66	0.9	2.1
MAU-09	20	12.9	1.15	3443	0.68	193	1.14	323	100.0	118.1	11.2	11.79	0.12	100	1.2	1.6
MAU-10	20	29.3	1.16	3490	1.55	325	2.72	572	99.9	113.9	8.4	12.23	0.12	97	1.1	1.8
MAU-11	20	11.1	1.14	3425	0.66	156	0.97	231	100.0	132.7	14.1	12.48	0.24	26	1.2	1.9
MAU-14	20	16.9	1.17	3508	1.96	412	1.66	349	99.7	235.7	18.1	11.22	0.17	55	1.3	1.7
MAU-15	20	14.4	1.14	3434	0.84	231	1.30	356	98.1	127.8	11.3	11.58	0.15	45	1.0	1.7
MAU-16	20	13.9	1.14	3415	0.58	123	1.22	260	97.5	93	10.4	12.10	0.20	43	1.3	1.9
MAU-22	20	8.4	1.16	3471	0.37	93	0.82	206	100.0	90.2	11.5	12.14	0.30	22	1.4	1.6
MAU-23	20	18.0	1.17	3517	0.75	189	1.51	382	24.9	100.7	10.1	11.45	0.31	25	1.6	1.6

Note. $\rho_{i,s,d}$ are track density of induced, spontaneous, and dosimeter track counts, respectively. $N_{i,s,d}$ are number of induced, spontaneous, and dosimeter track counts, respectively. P is the value of the chi-square (χ^2) age homogeneity test. 1σ is the error calculated using the Zeta calibration technique ($\zeta = 348.18 \pm 6.5$). MTL is the mean track lengths. SE is the standard error. SD is the standard deviation. D_{par} are measurements of etch pit diameter used as proxy for chemical composition influence on track annealing.

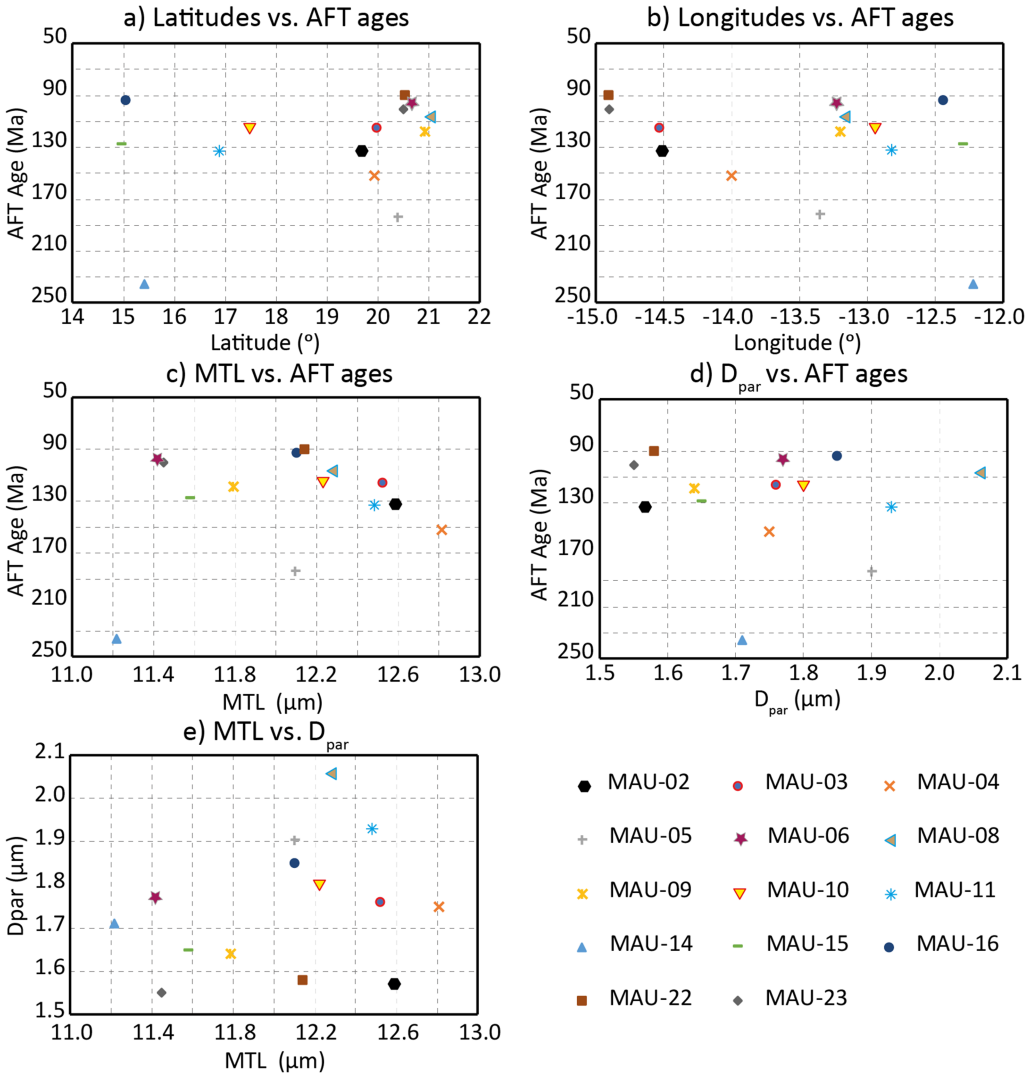

Figure 2. Plots of AFT central ages against (a) sample latitude, (b) longitude, (c) track lengths, and (d) mean D_{par} values. (e) Plot of mean track lengths against mean D_{par} values. MTL: mean track lengths.

4. Analytical Results

4.1. Apatite Fission Tracks

The AFT data are reported in Table 2 and show AFT central ages ranging between 235.7 ± 18.1 and 90.2 ± 11.5 Ma. All the samples passed the chi-square test (i.e., P(χ^2) >5 %), which indicates an insignificant single-grain age dispersion (Table 2). Eleven samples out of fourteen indicate Cretaceous cooling with Hauterivian to Campanian AFT ages. The remaining three samples yielded two Jurassic ages (MAU-04 and MAU-05) and one Late Triassic age (MAU-14). There is no apparent correlation between the spatial distribution of the samples and their AFT ages (Figure 2a and b). Track lengths were measured in all samples and, typically, the aim is to measure a minimum of 100 confined tracks per sample when possible (Donelick et al., 2005). Track length distribution in samples with low number of measurements, which is primarily attributed to relatively low uranium content (Table 2), should be interpreted with caution. Most samples show unimodal track length distributions with mean track lengths varying from 11.22 to 12.81 μm (Figure 3). Although there is no correlation between AFT ages and mean track lengths (Figure 2c), the sample with the oldest AFT age (i.e., MAU-14: 235.7 ± 18.1 Ma) is characterized by the shortest mean track length (i.e., 11.22 ± 0.17 μm). It suggests that prior to the Cretaceous cooling event, most samples experienced annealing. Track annealing may be influenced by apatite composition (e.g., Barbarand et al., 2003), which can skew the mean track length-age relationship. D_{par} measurements, used as proxy for compositional influence on

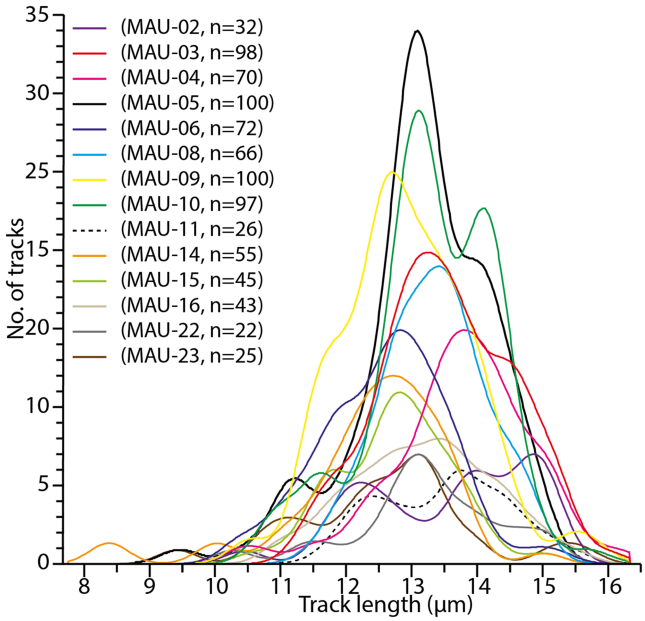

Figure 3. Density plot showing track length distribution for each sample.

apatite annealing kinetics, are comprised between 1.6 and 2.1 μm, and show no correlation with AFT ages and mean track lengths (Figure 2d and e).

4.2. Apatite (U-Th-Sm)/He

Three to four apatite aliquots from nine samples were successfully analysed (32 aliquots in total). The AHe data, the uncorrected, and corrected ages are summarized in Table 3. Since there is a complex relationship between α-ejection, radiation damage (of U, Th, and Sm), and He diffusion (e.g., Gautheron et al., 2012), the usage of the Ft factor can result in over-corrected AHe ages. Thus, we use uncorrected AHe ages to describe and analyse the obtained results. The correction for α-ejection is treated during the thermal modelling presented in the next section. The oldest aliquot age of 261.3 ± 4.6 Ma is obtained from sample MAU-14 and the youngest aliquot age of 33.7 ± 1.4 Ma is obtained from sample MAU-16. The mean uncorrected AHe ages range from 158 ± 95.4 to 50.1 ± 19.7 Ma. Samples MAU-09, MAU-15, and MAU-23 show a good reproducibility of single aliquot ages, with standard deviations of less than 15 %, whereas samples MAU-14 and MAU-22 show a high single age dispersion with standard deviations of more than 50 %. AHe age dispersion is primarily the result of the thermal history of the samples, radiation damage within the apatite crystal, and/or variation in the size of the analysed grains (e.g., Brown et al., 2013; Fitzgerald et al., 2006; Gautheron et al., 2012). To assess the influence, if any, of these factors, we examine the relationship between single aliquot ages, eU content (used as proxy for radiation damage), and crystal spherical equivalent radius (R^*). Graphs in Figure 4 show that samples MAU-04, MAU 05, MAU-16, and MAU-22 have a clear positive age-R^* correlation, while samples MAU-05 and MAU-15 display a strong positive age-eU correlation. Thus, the large age dispersion could be related to the size of the analysed aliquots in the case of MAU-22, whereas it is probably due to the combined effect of several factors in the case of MAU-14.

All AHe average uncorrected ages are younger than the respective AFT central ages (Figure 5). While, most of them indicate a main cooling event through the apatite partial annealing zone during the Late Cretaceous to Eocene, two samples suggest an older Late Jurassic–Early Cretaceous cooling event (MAU-04 and MAU-14; Figure 5 and Table 3).

5. Inverse Thermal Modelling

5.1. Modelling Approach

The interpretation of the AFT and AHe results requires the integration of both datasets using an adequate time-temperature (t-T) inversion method to account for the obtained ages, track lengths, composition (i.e., D_{par}), and related uncertainties. To this purpose, we use the inverse modelling software QTQt, which is based on the Bayesian transdimensional Markov Chain Monte Carlo (MCMC) method described in Gallagher

Journal of Geophysical Research: Solid Earth

10.1029/2019JB017914

Table 3
Results of (U-Th-Sm)/He analysis

											Uncorrected age				Ft-Corrected age			
Sample	Aliquot	^{4}He	^{238}U [ppm]	^{232}Th [ppm]	^{147}Sm [ppm]	eU [ppm]	Length [μm]	Width [μm]	R* [μm]	Age [Ma]	± AU [Ma]	Mean [Ma]	SD [Ma]	Ft	Age [Ma]	± 2σ [Ma]	Mean [Ma]	SD [Ma]
	1	1.33E+00	21.3	3.9	129.5	22.2	190.0	101.3	53.2	92.1	1.9			0.71	130.7	12.7		
	2	8.19E-01	26.5	7.7	153.3	28.3	157.8	101.3	51.9	63.6	1.3			0.69	91.9	9.3		
	3	5.31E-01	19.5	5.3	135.7	20.8	161.7	98.2	56.5	55.6	1.2			0.73	76.3	7.0		
MAU_03	4	9.63E-01	21.1	4.1	148.0	22.1	146.5	125.2	57.2	80.1	1.6	72.9	16.4	0.71	112.9	10.8	102.9	23.8
	1	1.62E+00	58.9	26.7	235.4	65.2	197.3	80.8	45.3	82.5	1.6			0.64	128.9	14.8		
	3	6.26E-01	39.1	15.4	91.8	42.7	115.2	76.9	43.8	92.5	2.1			0.65	141.7	16.1		
MAU-04	4	2.14E+00	18.4	29.5	88.4	25.4	187.3	116.5	60.1	132.6	2.4	102.5	26.5	0.73	180.4	15.7	150.3	26.8
	1	1.77E-01	19.2	9.7	323.5	21.5	118.0	73.6	42.8	45.6	1.2			0.64	71.6	8.7		
	2	7.09E-01	36.0	17.2	353.0	40.0	113.5	101.0	55.4	70.0	1.4			0.72	97.3	9.0		
MAU-05	4	1.57E-01	19.0	9.4	250.8	21.2	128.2	60.8	36.3	44.9	1.4	53.5	14.3	0.58	78.0	11.0	82.3	13.4
	1	7.57E-01	29.4	83.2	409.4	48.9	141.3	82.6	42.2	67.8	1.3			0.62	109.9	13.3		
	2	1.41E+00	14.6	46.5	751.6	25.5	152.6	125.2	59.2	67.8	1.2			0.72	94.2	8.6		
	3	2.01E+00	28.1	81.9	407.9	47.3	153.9	101.3	58.5	72.3	1.3			0.72	100.0	9.0		
MAU-09	4	4.34E+00	79.4	195.8	613.9	125.4	190.4	101.3	54.3	73.8	1.2	70.4	3.1	0.70	104.8	9.9	102.2	6.7
	1	3.24E-01	17.1	6.5	304.8	18.6	110.8	81.7	40.1	78.5	2.1			0.59	132.9	17.8		
	2	6.24E-01	22.0	4.3	245.0	23.0	163.0	81.7	47.9	75.3	1.6			0.68	110.4	11.5		
	3	1.04E+00	18.4	6.4	272.5	19.8	131.3	75.6	39.6	216.7	5.2			0.58	376.7	51.3		
MAU-14	4	3.05E+00	28.3	64.5	329.5	43.5	118.2	98.7	46.9	261.3	4.6	158.0	95.4	0.65	399.9	43.9	255.0	154.5
	1	5.42E-01	30.2	15.1	238.1	33.8	151.7	70.9	42.4	82.2	1.8			0.61	134.4	16.8		
	2	4.94E-01	22.8	10.7	178.4	25.3	141.3	84.8	60.1	71.4	1.6			0.76	93.7	7.8		
MAU-15	3	5.30E-01	36.5	21.2	259.5	41.4	113.9	71.7	41.7	82.8	1.8	78.8	6.4	0.63	132.2	15.9	120.1	22.9
	1	6.68E-01	17.7	7.3	67.3	19.5	187.3	144.7	70.8	72.0	1.5			0.76	94.8	7.9		
	2	1.33E-01	8.2	7.0	49.7	9.8	144.7	91.3	59.3	44.7	1.7			0.73	61.2	6.7		
MAU-16	3	7.17E-02	10.9	12.2	44.4	13.7	135.2	62.6	43.3	33.7	1.4	50.1	19.7	0.67	50.5	6.5	68.8	23.1
	1	1.09E+00	11.6	5.9	206.5	13.0	141.7	116.9	63.7	148.0	3.1			0.79	188.4	14.5		
	2	5.37E-01	6.6	2.9	188.1	7.2	236.5	107.4	58.3	74.0	1.6			0.74	100.4	9.1		
	3	1.62E-01	7.3	6.1	226.0	8.8	120.0	91.3	44.3	57.3	1.9			0.64	89.1	11.2		
MAU-22	4	3.25E-01	13.2	6.3	241.2	14.7	172.1	87.8	46.8	50.4	1.2	82.4	44.8	0.65	77.1	8.8	113.8	50.7
	1	4.12E+00	72.2	29.3	91.6	79.0	173.1	114.3	66.0	73.1	1.4			0.77	95.5	7.6		
	2	2.17E+00	45.0	42.7	64.8	55.0	116.0	123.7	66.2	78.5	1.4			0.75	104.3	8.6		
	3	2.70E-01	23.8	22.8	24.4	29.1	165.4	98.4	51.3	58.1	1.6			0.69	84.8	9.3		
MAU-23	4	4.11E-01	10.2	2.4	19.3	10.8	165.8	121.7	69.3	69.1	1.6	69.7	8.6	0.77	89.3	7.3	93.5	8.4

Note. eU is effective Uranium content calculated as $eU_{ppm} = [U_{ppm}] + 0.235 \times [Th_{ppm}]$. R* is crystal spherical equivalent radius calculated as $R^* = (3 \times (R \times L))/(2 \times (R + L))$ and where L is crystal length, W is crystal width, and R = W/2. AU is analytical uncertainty calculated by adding analytical procedure error and standard deviation of the reproducibility of Durango apatite standards. SD is the standard deviation of the calculated mean age. Ft is α-ejection correction, calculated to account for α-particle loss in the outer 20 μm of the apatite crystal (Farley et al., 1996).

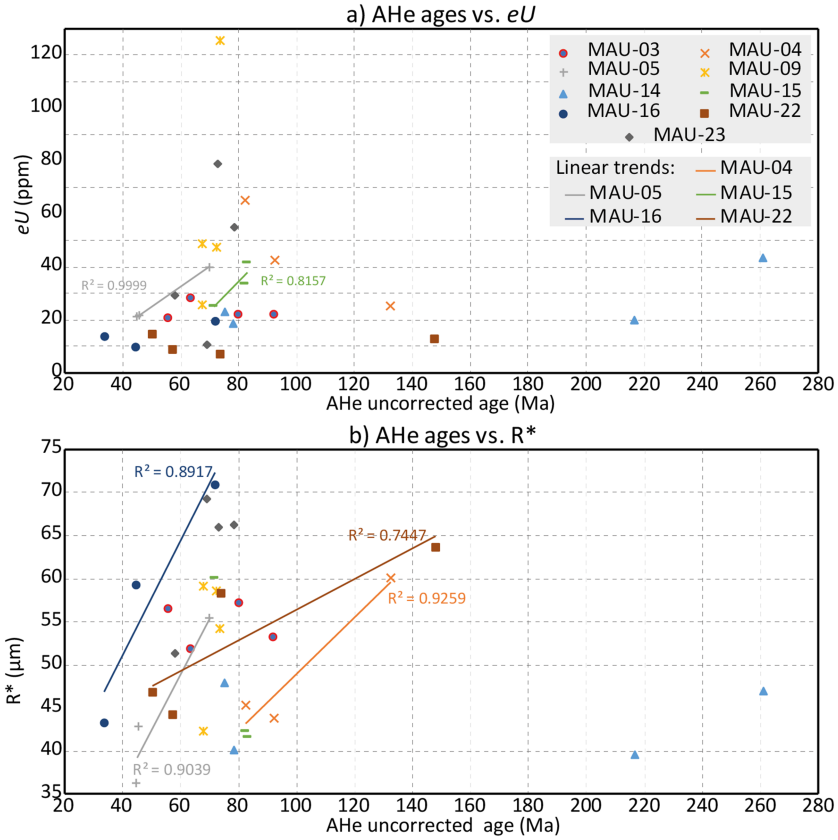

Figure 4. Plots of AHe aliquot ages (uncorrected) against (a) the effective Uranium content (eU) and (b) the crystal spherical equivalent radius (R^*). eU_{ppm} = [Uppm] + 0.235 x [Th_{ppm}]. R^* = (3 x (R x L))/(2 x (R + L)), where L is crystal length, W is crystal width, and R = W/2. Linear correlation trend is shown for samples with a good correlation coefficient ($R^2 > 0.7$).

(2012). QTQt allows for the examination of a large range of possible t-T paths and provides probability distribution and predicted ages (i.e., AFT and AHe), track length distribution, and Dpar of the sampled paths (Cogné et al., 2011; Fitzgerald et al., 2006; Gallagher, 2012; Gallagher and Ketcham, 2018; Gallagher et al., 2009; Vermeesch & Tian, 2014).

We model the thermal history of samples MAU-03, MAU-09, MAU-10, MAU-14, and MAU-15 which cover the full extent of the sampled area. AHe single aliquot ages were jointly inverted with the corresponding AFT data, except for sample MAU-10, which AHe analysis was unsuccessful. The correction for α-particle ejection is constrained by the dimensions of each aliquot (Farley et al., 1996) and accounted for at each time step during the inversion (see Gallagher, 2012). The inversions were run for 1,000,000 iterations after discarding the initial 'burn in' of 50,000 iterations (Gallagher, 2012), and were based on the AFT annealing kinetics of Ketcham et al. (2007) and the He kinetics of Flowers (2009). The effect of apatite composition on fission track annealing was approximated by the average D_{par} value of each grain (Barbarand et al., 2003; O'Sullivan and Parrish, 1995).

5.2. Geological Constraints

The samples were taken from Precambrian granitic bodies that intruded the Archean–Palaeoproterozoic basement of the West African Craton during the Pan-African Orogeny (ca. 900–500 Ma; Black and Liegeois, 1993; Li et al., 2008). Pan-African rocks together with Palaeozoic sediments (belonging to the Taoudeni Basin in the east) are found deformed and metamorphosed along the Mauritanide belt (Villeneuve, 2005). This suggests that our samples were buried underneath the Palaeozoic sediment of the Taoudeni Basin (up to 6 km thick), then were exhumed during the Variscan Orogeny leading to the build-up of the Mauritanides (ca. 330–270 Ma; Villeneuve, 2005). To account for this evolution, two geological constraints were used for

the thermal history inversion: an initial constraint at 350 ± 20 Ma/120 ± 20 °C (burial before the Variscan Orogeny) and a second constraint at 300 ± 30 Ma/50 ± 30 °C (exhumation during the Variscan Orogeny).

5.3. Modelling Results

The results of the thermal inversions are shown in Figures 6 and 7. The probability distribution in time-temperature (t-T) space is based on all sampled t-T paths. The weighted mean model, called the expected model, is weighed according to the probability of each sampled t-T path. The uncertainty associated with the expected model is represented by the 95 % probability range (Gallagher, 2012).

The expected Palaeozoic t-T paths of all samples predict an initial cooling from 90–110 to 70–60 °C by 290 Ma, which is consistent with the imposed two constraints (Figure 6). During post-Variscan times (ca. < 270 Ma), samples MAU-03, MAU-10, and MAU-15 yielded identical t-T pattern with two heating phases and two cooling phases (Figure 6a, c, and e). During the initial heating, MAU-03 and MAU-10 reached 100 °C by 180 and 165 Ma, respectively, while MAU-15 reached 80 °C by 215 Ma. The following cooling phase lasted until 75–55 Ma when the three samples reached 40–30 °C. In the last heating, the samples were heated by 15–20 °C to reach 60–50 °C by 15 Ma. The final cooling brought the samples to the surface (i.e., 20 °C), their present-day elevation. Sample MAU-09 also shows two post-Variscan heating and cooling events, but its expected t-T path suggests an isothermal period at ca. 90 °C that lasted 50 Myr between 210 and 160 Ma (Figure 6b). It was followed by a very slow heating to 80 °C by 90 Ma, then a rapid ca. 60 °C cooling within 10 Myr. The last recorded heating phase brought the sample from 20 to 55 °C and lasted from 100 to 15 Ma, before it reached present-day surface temperature after a final cooling event. Sample MAU-14, on the other hand, shows a much simpler expected thermal evolution, with a continuous cooling that started during Variscan times. The cooling rate was initially extremely slow at 0.07 °C/Myr but increased suddenly at 15 Ma to 2 °C/Myr. To assess the robustness of the inverse modelling of MAU-14 and the significance of the predicted thermal history, we forward modelled a t-T path matching the trend shown by the other four models (Figure 8a).

The predicted AFT ages, AHe ages, and track length distribution are in agreement with observed data. The forward model suggests that a thermal history similar to predictions obtained from the other four samples is possible.

The predicted heating and cooling events occur at relatively low rates (i.e., < 0.6 °C/Myr), except the 6 °C/Myr cooling recorded by MAU-09 between 90 and 100 Ma, and the last cooling event (15-0 Ma), recorded in all samples at 2–3 °C/Myr.

Overall, the t-T paths, predicted by inverse modelling, or forward modelling in the case of MAU-14, suggest a relatively coherent thermal history along the entire Mauritanian margin (Figure 9a). Cooling events occurred during the Variscan time (ca. 350-290 Ma), the Late Jurassic–Early Cretaceous (ca. 160–95 Ma), and the mid-Miocene–Present (ca. 15–0 Ma), while heating events took place during the Permo-Triassic (ca. 290–200 Ma) and the Paleocene–mid-Miocene (ca. 60–15 Ma) (Figure 9a).

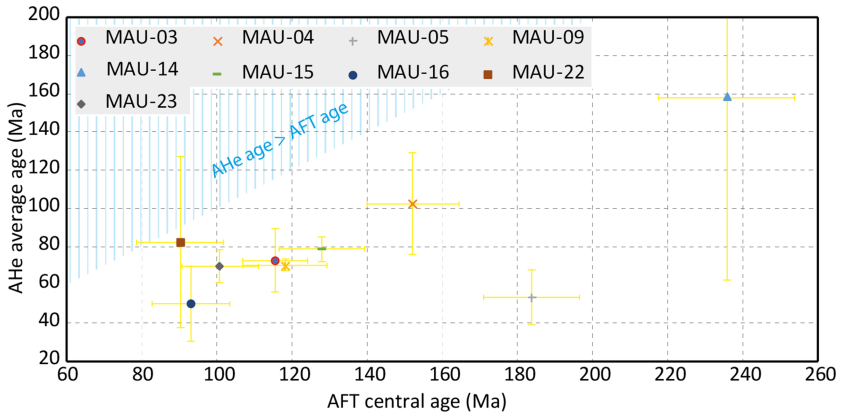

Figure 5. Plot of AFT central age against AHe average age (uncorrected). Yellow bars indicate the error, which is 1σ for the AFT ages and the standard deviation for the AHe ages.

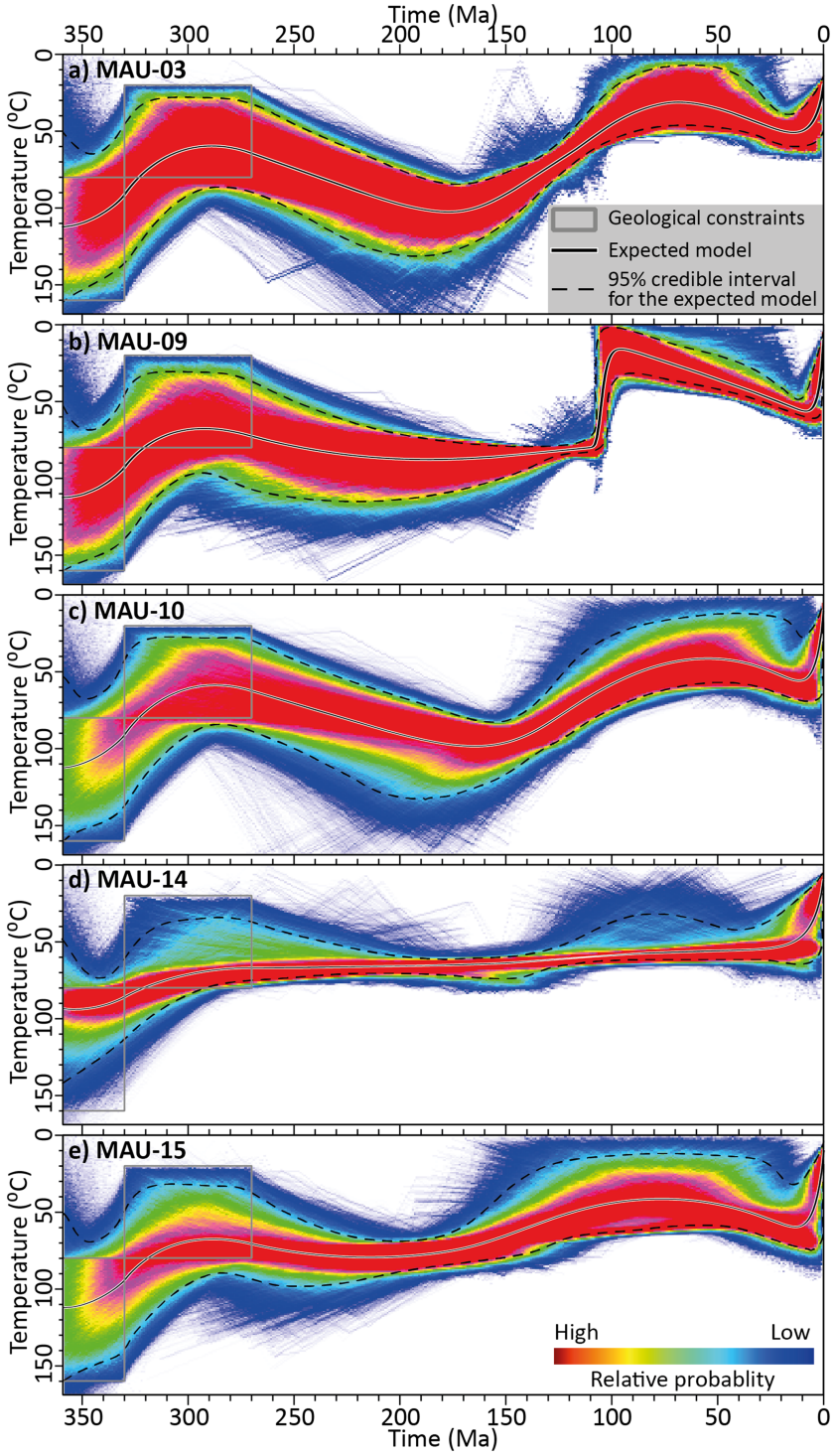

Figure 6. Thermal inverse modelling results constrained by AFT and AHe data of samples a) MAU-03, b) MAU-09, c) MAU-10, d) MAU-14, and e) MAU-15. The graphs show the expected t-T path (black line with white outline) and probability distribution of sampled thermal histories. Grey boxes are the imposed geological constraints.

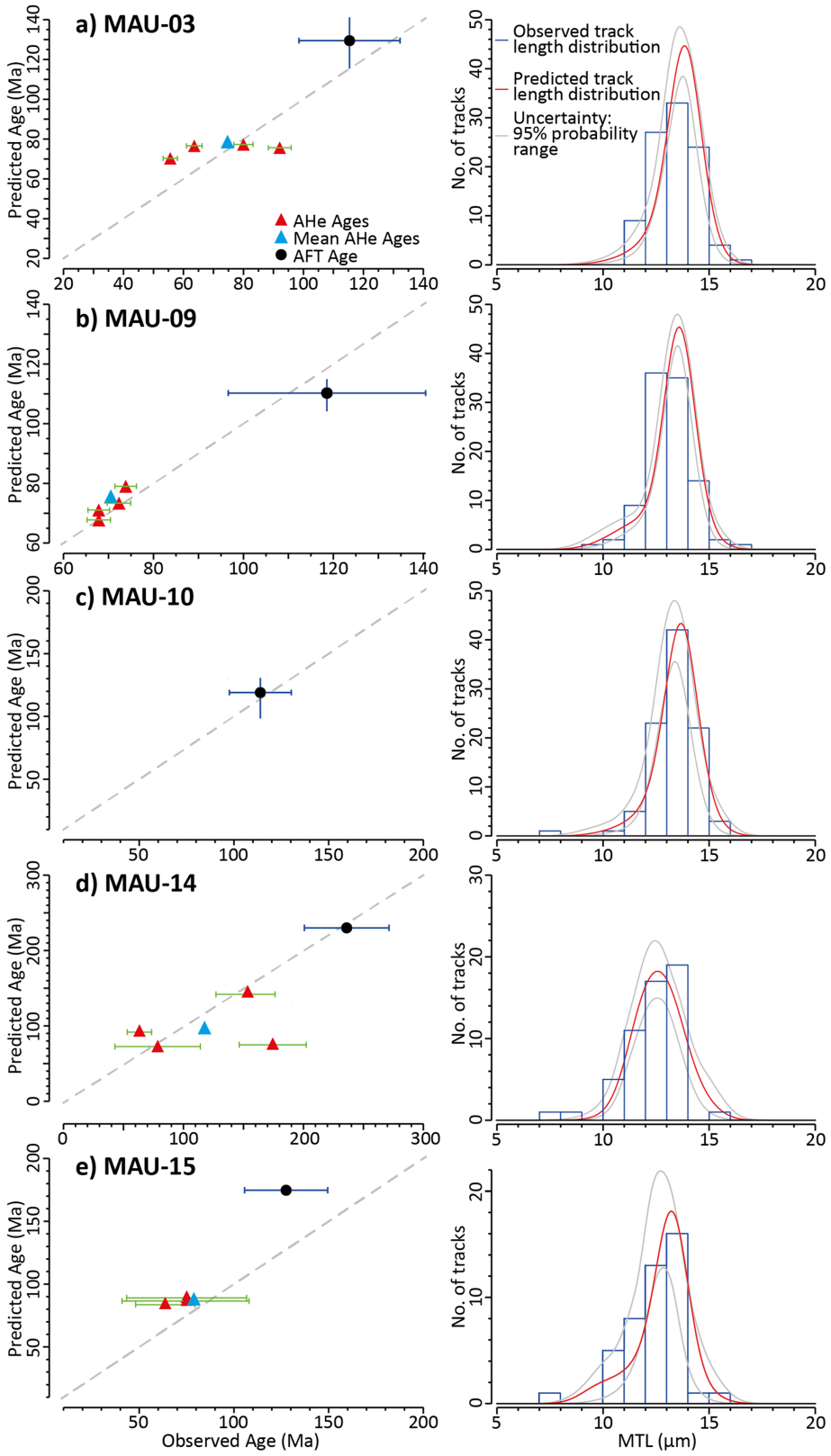

Figure 7. Thermal inverse modelling results constrained by AFT and AHe data of samples a) MAU-03, b) MAU-09, c) MAU-10, d) MAU-14, and e) MAU-15. Predicted AFT and AHe ages (left), and apatite track length distributions (right).

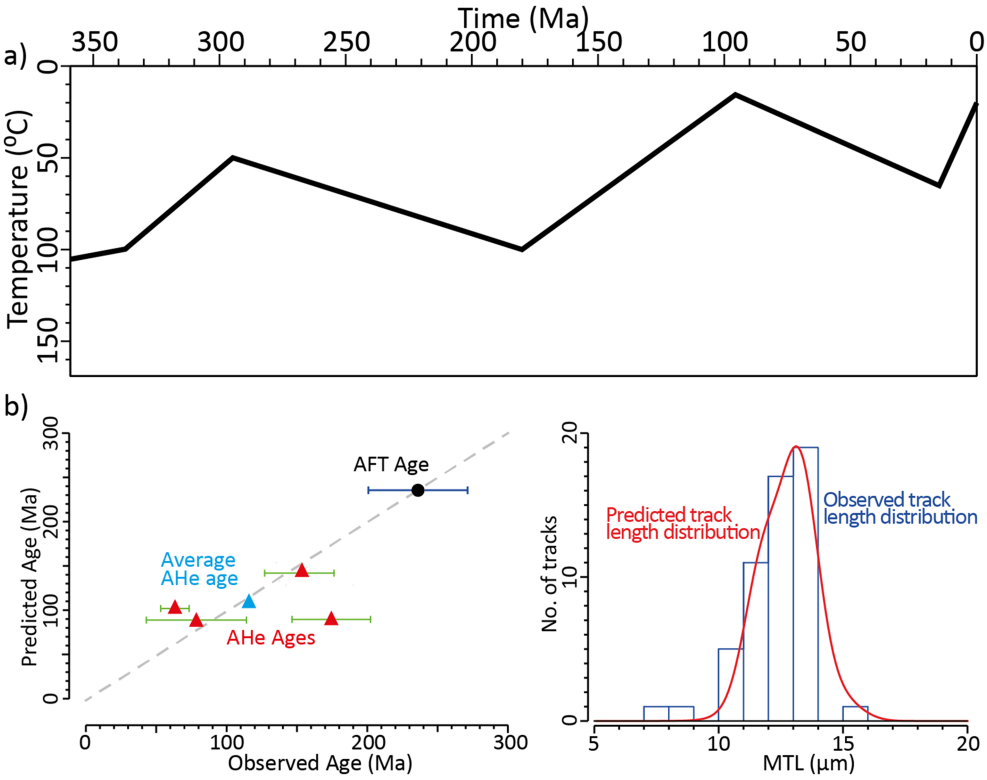

Figure 8. Forward thermal modelling of sample MAU-14. a) Forward modelled t-T path. b) Predicted AFT ages, AHe ages, and track length distribution.

6. Discussion

According to LTT, domains in the hinterland of the NW African margin, where Palaeozoic and/or Precambrian basement is exposed (e.g., the Reguibat Shield to the north of Mauritania, the Anti-Atlas belt, the High Atlas of Marrakech, and the Western Meseta in Morocco), show several cooling and heating events during Mesozoic and Cenozoic times (e.g., Ghorbal et al., 2008; Gouiza et al., 2017, 2018; Leprêtre et al., 2015; Ruiz et al., 2011; Saddiqi et al., 2009; Sehrt et al., 2017). Mesozoic to Cenozoic thermal events are also documented by the few LTT studies carried out onshore the conjugate North American margin (Lorencak et al., 2004; RodenTice & Tice, 2005; RodenTice & Wintsch, 2002; RodenTice et al., 2000; Spotila et al., 2004; Taylor & Fitzgerald, 2011).

These thermal events, interpreted as vertical movements of the Earth's surface (i.e., subsidence/burial and exhumation/denudation), were somehow linked to the evolution of the Central Atlantic Ocean (Gouiza et al., 2018; Leprêtre et al., 2017; Sehrt et al., 2018; Teixell et al., 2009). Hereafter, we discuss our new findings along the Mauritanian margin, their uncertainties, and their link to the regional geodynamic context, which is argued to largely contribute to the post-Variscan vertical movements documented in the Central Atlantic realm.

6.1. Uncertainties and Limitations

When modelling thermochronology data, there are uncertainties related to the analytical errors in the observed data, the choice of the kinetic models (FT annealing and α-damage models), and the imposed constraints. The analytical errors are used alongside the input data in the QTQt modelling. They are taken into account in modelling AFT and AHe data and the probability weighting of tested t-T paths. The kinetic models are built on simplifications, assumptions, and calibrations, which uncertainty is beyond the scope of this contribution (see Flowers et al., 2009; Gautheron et al., 2012; Ketcham et al., 2007). Nonetheless, to assess the sensitivity of our data to the He-diffusion model used in the QTQt modelling, we ran simulations using the α-damage model from Gautheron et al. (2012). The thermal inversion results (Figures S1 and S2 in the supporting information) indicate that both He-diffusion models (i.e., Flowers, 2009; Gautheron et al.,

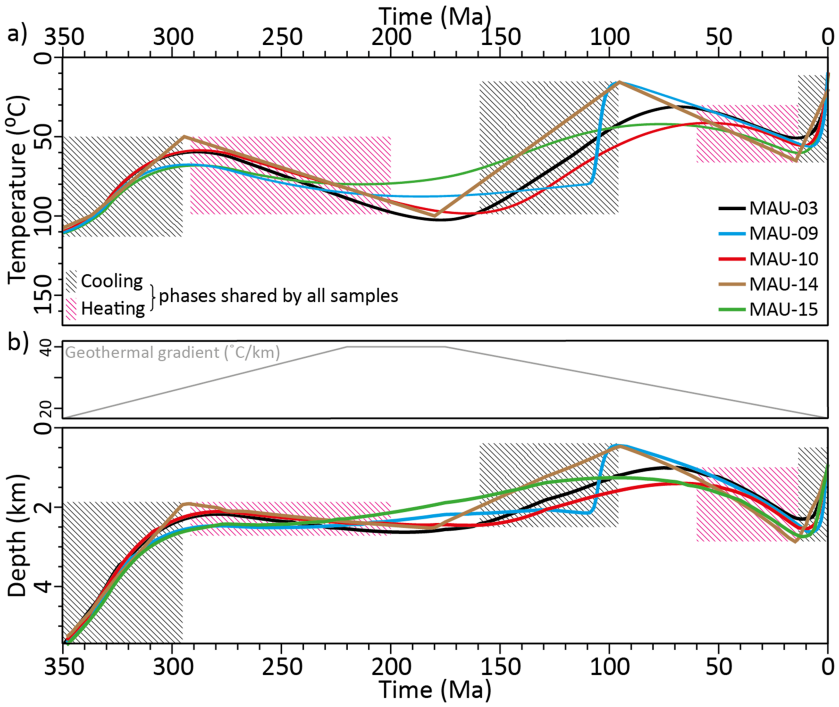

Figure 9. a) Expected thermal histories predicted by the inverse modelling of samples MAU-03, MAU-09, MAU-10, and MAU-15, and by the forward modelling of sample MAU-14. b) Vertical movements calculated from the expected t-T paths using a geothermal gradient of 20 °C/km except between 220 and 145 Ma where a geothermal gradient of 40 °C/km was applied to account for the effect of the Atlantic rifting. The dashed boxes indicate cooling/exhumation (black) and heating/burial (pink) phases shared by all the t-T paths.

2012) yield comparable expected t-T paths. We also tested the sensitivity of the models to the imposed geological constraints by running geologically unconstrained thermal inversions. The obtained expected t-T paths (Figure S3 and S4 in the supporting information) indicate that the samples remained at high temperatures between 110 and 80 °C during most of the Palaeozoic, which is in contradiction with the orogenic event recorded in the Mauritanides (ca. 330–270 Ma; Villeneuve, 2005). The predicted post-Triassic thermal histories on the other hand are very similar to the ones in the constrained models (Figure S4).

Low track length count ($\ll 100$) also introduces some uncertainty in the thermal inversion and the modelled track length distribution in particular. Thus, the modelling predictions obtained from MAU-03, MAU-09, and MAU-10, which have 97 to 100 measured track lengths, are considered more robust than the thermal histories obtained from MAU-14 and MAU-15, which have only 55 and 45 measured track lengths, respectively.

Another major uncertainty when quantifying vertical movements constrained by LTT data is the assumption on the palaeo-geothermal gradient, especially in tectonically active domains where the geothermal gradient varies spatially and/or temporally. These variations could be attributed to shallow processes like denudation, burial, and fluid circulations, but also to deep processes like magmatism, variations in crustal radiogenic heat, and changes in the basal heat (i.e., at the lithosphere-asthenosphere boundary) (e.g., Ehlers, 2005; Mareschal and Jaupart, 2004). Present-day values of the geothermal gradient in the West African Craton are very low ranging between 10 and 16 °C/km, which is consistent with values in old cratons (Rimi, 2000; Rimi, 1999). These values increase substantially in the Palaeozoic basins found within the craton and the Mesozoic coastal basins (e.g., 20–30 °C/km; Rimi, 1990). Our samples were taken along the western boundary of the West African Craton, which formed the eastern flank of the Triassic to Early Jurassic Atlantic rift (e.g., Davison, 2005). The flanks of active rifts (e.g., East African and Rhine rifts) show a relatively elevated surface heat flow (i.e., 52–73 mW/m^2; Kusznir and Park, 1987). Thus, to account for the thermal effect of the Atlantic rifting, we adopted a geothermal gradient of 40 °C/km between 220 and 175 Ma (i.e., syn-rift period; Davison, 2005), which linearly decreases to 20 °C/km by 350 Ma and 0 Ma (Figure 9b).

6.2. Post-Variscan Vertical Movements Along Central Atlantic Margins

Following the Variscan Orogeny, during the Permian and Triassic (ca. 290–220 Ma), possibly the Early Jurassic as well (ca. 180 Ma), the sampled rocks were heated by 20 to 50 °C. The amount of burial is estimated at ca. 0.6 to 1 km (Figure 9). A coeval burial event is documented in the Western Meseta (Ghorbal et al., 2008; Saddiqi et al., 2009) and the central and eastern Reguibat Shield (Leprêtre et al., 2017). In the Moroccan Western Meseta, Ghorbal et al. (2008) suggest up to ca. 4 km of burial during the Triassic and the Jurassic. While Saddiqi et al. (2009) suggest ca. 2 km of burial during the Triassic and Early Jurassic. In the Reguibat Shield, the central and eastern parts underwent also a burial of up to ca. 2 km during the Permian, Triassic, and Early Jurassic according to Leprêtre et al. (2017). On the conjugate margin, the southern Canadian Shield terranes show a heating phase during the Permian and Triassic with ca. 2 km of burial (Lorencak et al., 2004).

The first cooling event along the Mauritanian margin started around the Middle Jurassic (ca. 180–160 Ma) and continued until the Late Cretaceous (ca. 100 Ma). The samples cooled by about 80 °C, which corresponds to ca. 2 km of exhumation (Figure 9). A similar exhumation event is reported by LTT studies in other domains along both sides of the Central Atlantic. In the Moroccan Meseta, the exhumation started around the Early-Middle Jurassic and ended by the late Early Cretaceous (ca. 120–100 Ma). In the High Atlas of Marrakech, exhumation initiated much earlier during the Devonian–Carboniferous (ca. 400–350 Ma) and continued until the end of the Early Cretaceous (Balestrieri et al., 2009). In the Reguibat Shield, exhumation occurred during the Jurassic and stopped by the beginning of the Early Cretaceous (ca. 130 Ma), except in the eastern part where it continued until the present-day (Leprêtre et al., 2017). Overall, all these domains show between 2.5 and 4 km of exhumation between the Middle Jurassic and the Late Cretaceous when Precambrian to Palaeozoic rocks were exhumed from relatively high temperatures (ca. 120–90 °C) to surface (or near surface) temperatures (ca. 30–15 °C). In contrast, stratigraphic records from sedimentary basins on the shelf and the coastal domain of the Central Atlantic margins show an almost uninterrupted subsidence between the Middle Jurassic and the Cretaceous. Carbonate platform build-up which started in the Middle Jurassic (or earlier) continued until the Early Cretaceous when siliciclastic systems started developing along both sides of the Central Atlantic (e.g., Davison, 2005).

A second phase of heating by 15 to 30 °C occurred during the Paleocene to mid-Miocene (ca. 60–15 Ma), which indicate a 0.7 to 1.5 km of burial (Figure 9). A coeval burial event with similar magnitude is documented in the Moroccan Meseta (Ghorbal et al., 2008; Saddiqi et al., 2009), the High Atlas of Marrakech (Balestrieri et al., 2009), and the western and central Reguibat (Gouiza et al., 2018; Leprêtre, 2015; Leprêtre et al., 2014).

The last cooling event, illustrated by the t-T models, occurred between the mid-late Miocene and the Present (ca. 15–0 Ma). The samples cooled by about 30 to 50 °C, thus, indicating ca. 1.5 to 2.5 km of exhumation (Figure 9). A comparable exhumation event is documented in pre-Mesozoic terranes in Morocco like the Western Meseta, the High Atlas of Marrakech, and the Reguibat Shield (Balestrieri et al., 2009; Ghorbal et al., 2008; Gouiza et al., 2018).

Samples from the southern Canadian Shield and the Appalachian Adirondack mountains, on the conjugate East American margin, suggest a prolonged phase of exhumation during most of the Mesozoic and Cenozoic (Lorencak et al., 2004; RodenTice and Tice, 2005; RodenTice et al., 2000; Taylor and Fitzgerald, 2011). There are no evidences of the Late Cretaceous to mid-Miocene heating documented along the Mauritanian and other NW African margins.

6.3. Tectonic and Geodynamic Processes

The Permo-Triassic and Early Jurassic heating/burial event coincides with continental rifting and lithospheric thinning that led to the opening of the Central Atlantic in the Early Jurassic (e.g., Davison, 2005; Le Roy and Piqué, 2001; Sahabi et al., 2004). Several major rift basins are found above the present-day sea level between the Moroccan and Senegalese margins (e.g., Doukkala Basin, Essaouira Basin, Tarfaya-Dakhla Basin, Mauritanian-Senegalese Basin). They indicate that tectonic subsidence related to the Atlantic rifting was widely distributed and extended farther east, beyond the present-day shoreline. Our results suggest that the Mauritanides in Mauritania experienced up to 1 km of burial. The lack of syn-rift structures and Triassic to Lower Jurassic syn-rift sediments east of the coastal basin, suggest that it is unlikely that tectonic subsidence reached the western margin of the West African Craton. Nevertheless, burial rates derived from the expected thermal models are between 6 and 18 m/Myr. They are comparable with minimum subsidence

rates calculated in well data from the shelf and coastal basins of the Moroccan margin (Gouiza, 2011; Gouiza et al., 2010; Le, 1997). It is also possible that this heating event could be partly explained by a very high geothermal gradient. As discussed above, we already assume a geothermal gradient of 40 °C/km during the Late Tiassic–Early Jurassic (220–175 Ma) to account for the thermal effect of the Atlantic rift. However, if we assume an even higher geothermal gradient of 80 °C/km, proposed for some rift basins (e.g., Malusà et al., 2016), the amount of burial would be reduced to 0.6 km.

The process (or processes?) driving the Jurassic to Cretaceous cooling is more intriguing, as it needs to reconcile the km-scale exhumation of the hinterlands of both sides of the Atlantic with the contemporaneous subsidence in the surrounding basins. It has also to account for the large E-W wavelength of the exhumation event, which affected domains extending over 600 km (e.g., the Reguibat Shield). Authors have already proposed deep processes like mantle plume underneath the entire Central Atlantic (Leprêtre et al., 2017) or small-scale mantle convection cells (Gouiza, 2011). A rising hot asthenosphere plume underneath the Central Atlantic during the Jurassic to Cretaceous time, as suggested by Leprêtre et al. (2017), can explain the long-lived exhumation event. It, however, can neither account for the concurrent subsidence in the shelf and coastal basins nor the N-S wavelength of the exhumation. Gouiza (2011) examined the effect of edge-driven small-scale convective cells that would initiate at the base of the subcontinental lithospheric necking zone by the end of rifting. These localized convection cells can potentially reconcile between the exhumation and the subsidence observed on both conjugate margins. However, the thermo-mechanical modelling carried out by Gouiza (2011) predicts only few hundred meters of exhumation, which is in disagreement with the 2 km documented by LTT.

Regardless of the type of deep mantle process that was potentially involved, it can only partly explain the large Jurassic to Cretaceous cooling. Studies examining mantle-driven dynamic topography in oceanic realm suggest that the resultant elevation anomalies (positive or negative) do not exceed 1 km (Hoggard et al., 2017). Dynamic topography should be even less expressed in continental domains where the lithosphere is mechanically stronger (e.g., McKenzie et al., 2005). Alternatively, the Jurassic-Cretaceous exhumation could be primarily driven by a tectonic process with some contribution of mantle dynamics (if any). Especially since major geodynamic events, related to the evolution of the Atlantic domain, occurred during Jurassic to Cretaceous times. The Early Jurassic continental breakup in the Central Atlantic (e.g., Davison, 2005; Labails et al., 2010; Sahabi et al., 2004) and the Aptian–Albian (ca. 112 Ma) continental breakup in the South and North Atlantics (Torsvik et al., 2009; Tucholke et al., 2007) were key factors that controlled plate motion rate and direction. Thus, ultraslow spreading rates (ca. 0.5 to 2 cm/yr) are recorded at the beginning of the Middle Jurassic, which gradually increased to reach ca. 5.5 cm/yr by the Late Jurassic, and then suddenly dropped to ca. 3 cm/yr in the Early Cretaceous (Kneller et al., 2012; Labails et al., 2010; Schettino and Turco, 2009). The increase in spreading rate certainly increased the ridge push forces and the accumulated stress within the plates, which could have resulted in crustal- to lithospheric-scale folding (e.g., Cloetingh and Kooi, 1992; Ziegler and Cloetingh, 2004) and ultimately the reactivation of old basement structures (e.g., Boldreel and Andersen, 1998; Eagles and Wibisono, 2013). The decrease in spreading rate would then cause stress relaxation and can explain the minor burial event recorded between the Late Cretaceous and mid-Miocene.

The final Neogene cooling/exhumation phase is coeval with the uplift of many orogenic belts around the Mediterranean as a result of the Africa-Iberia/Europe convergence, which initiated in the Santonian (Martínez-Loriente et al., 2014). Stresses localized along the boundaries of the African plate, but also in its interior. Thus, deformation was accommodated along the northern boundary in the Rif-Tell system and in the interior of the plate in the Atlas system (Frizon De Lamotte, Bezar, Bracène, & Mercier, 2000). The Atlas fold-and-thrust belt experienced two major inversion phases, during middle-late Eocene to Oligocene then during late Miocene to Pliocene (Frizon De Lamotte et al., 2009). The latter phase coincides with the Neogene exhumation event revealed by LTT in NW Africa. The mobile belts around the WAC (e.g., Anti-Atlas and Mauritanides) were always interpreted as stable since the Variscan cycle (ca. 320–270 Ma; Ennih and Liégeois, 2008). Nonetheless, a recent field study by Soulaimani et al. (2014) showed that the Anti-Atlas owes its present elevation to the reactivation of Precambrian-Palaeozoic structures during the Atlas-Rif Orogeny. Our results hint that the Mauritanides structures might also have been reactivated during Neogene times.

6.4. Climate and Surface Processes

In addition to tectonic and geodynamic processes, the feedback between tectonic, climate, and surface processes can also influence the burial and exhumation history inferred from LTT (e.g., Allen, 2008; Braun, 2006). A provenance study by Ali et al. (2014) indicates that the detrital Cretaceous sediments in the coastal Tarfaya Basin, to the NW of the Reguibat Shield, were sourced from the Reguibat Shield and the Mauritanides. This suggests that basement material was eroded during the Middle Jurassic–Cretaceous cooling/exhumation event and was routed to the nearby subsiding basins. Since erosion can enhance or inhibit deformation and exhumation, such as high erosion rates localize deformation and promote exhumation (Braun, 2006), a change in climate can cause changes in the magnitude and rate of exhumation. NW Africa occupied mostly tropical latitudes during most of the Mesozoic (Müller et al., 2016); and general circulation models suggest that the climate was mostly dry and seasonally wet with significant precipitation during summer (Sellwood & Valdes, 2006). Although high erosion rates are not expected under dry conditions, Molnar (2001) postulated that in arid zones, an increase in relative magnitudes of rare floods or, conversely, an increase in the frequency of large floods can double erosion rates. Thus, it is possible that mantle dynamics and/or intra-plate stresses could have initially triggered the observed Jurassic to Cretaceous exhumation, which was then maintained and enhanced by climate-driven high erosion rates.

7. Conclusions

The new LTT data presented above indicate that the hinterland of the Mauritanian Atlantic margin underwent several thermal events during Mesozoic and Cenozoic times: (1) a heating event to 90–100 °C between the Permian and the Late Triassic (ca. 290–220 Ma); (2) a prolonged cooling event during Middle-Late Jurassic and Early Cretaceous (ca. 180–100 Ma); (3) a heating phase to 60–65 °C during the Palaeogene–early Miocene (ca. 60–15 Ma); and (4) a final rapid cooling event between the mid-Miocene and the present-day (ca. 15–0 Ma).

Our data are consistent with findings in the north, along the Moroccan Atlantic margin, where thermal events with comparable timing and magnitude were reported, and suggest episodes of burial and exhumation of the Earth's surface. Thus, the Permian–Late Triassic heating/burial is contemporaneous and linked to the Atlantic rifting and related tectonic subsidence. The following Middle-Late Jurassic and Early Cretaceous cooling/exhumation is coeval with major variations in spreading rates in the Central Atlantic. We suggest that the substantial increase in Central Atlantic spreading rate between the Late Jurassic and Early Cretaceous, was mirrored by an increase in intraplate stresses, which could have resulted in crustal- to lithospheric-scale folding and maybe the reactivation of basement structures in the Mauritanides. Stress relaxation, due to the decrease in spreading rate after the Early Cretaceous, could potentially explain the minor heating/burial episode during the Paleogene and early Miocene. The final cooling/exhumation recorded from the mid-Miocene to the present-day is associated with the Africa-Iberia/Europe convergence, which was mainly accommodated by the inversion of the Atlas-Rif system but its influence probably extended further south and affected the the West African Craton mobile belts (e.g., Anti-Atlas and Mauritanides).

Acknowledgments

This work was conducted in the frame of ongoing research on NW Africa funded by the North African Research Group (NARG) consortium. The fieldwork in Mauritania was only possible with the support of the Mauritanian Office for Geological Exploration (OMRG), in particular the managing director Mr El Hachemy Ould Sidaty and his adjunct Mr Abdellahi Ahmedou Bellal. We thank Mr Cheikh Lekbir for liaising with the OMRG and his hospitality during our stay in Nouakchott. This manuscript was greatly improved by critical reviews of two anonymous reviewers and the suggestions made by the Editor (Uri ten Brink) and Associated Editor (Mike Taylor). The low-temperature thermochronology data-sets produced in this work can be downloaded from the PANGAEA Data Repository (https://doi.pangaea.de/10.1594/PANGAEA.901278).

References

Ali, S., Stattegger, K., Garbe-Schönberg, D., Frank, M., Kraft, S., & Kuhnt, W. (2014). The provenance of Cretaceous to Quaternary sediments in the Tarfaya basin, SW Morocco: Evidence from trace element geochemistry and radiogenic Nd–Sr isotopes. *Journal of African Earth Sciences*, *90*, 64–76. https://doi.org/10.1016/j.jafrearsci.2013.11.010

Allen, P. A. (2008). From landscapes into geological history. *Nature*, *451*(7176), 274–276. https://doi.org/10.1038/nature06586

Baidder, L., Raddi, Y., Tahiri, M., & Michard, A. (2008). Devonian extension of the Pan-African crust north of the West African craton, and its bearing on the Variscan foreland deformation: Evidence from eastern Anti-Atlas (Morocco). *Geological Society, London, Special Publications*, *297*(1), 453–465. https://doi.org/10.1144/SP297.21

Balestrieri, M. L., Moratti, G., Bigazzi, G., & Algouti, A. (2009). Neogene exhumation of the Marrakech High Atlas (Morocco) recorded by apatite fission–track analysis. *Terra Nova*, *21*(2), 75–82. https://doi.org/10.1111/j.1365-3121.2008.00857.x

Barbarand, J., Carter, A., Wood, I., & Hurford, T. (2003). Compositional and structural control of fission-track annealing in apatite. *Chemical Geology*, *198*(1–2), 107–137. https://doi.org/10.1016/S0009-2541(02)00424-2

Bertotti, G., & Gouiza, M. (2012). Post-rift vertical movements and horizontal deformations in the eastern margin of the Central Atlantic: Middle Jurassic to Early Cretaceous evolution of Morocco. *International Journal of Earth Sciences*, *101*(8), 2151–2165. https://doi.org/10.1007/s00531-012-0773-4

Black, R., & Liegeois, J.-P. (1993). Cratons, mobile belts, alkaline rocks and continental lithospheric mantle: The Pan-African testimony. *Journal of the Geological Society*, *150*(1), 89–98. https://doi.org/10.1144/gsjgs.150.1.0088

Boldreel, L. O., & Andersen, M. S. (1998). Tertiary compressional structures on the Faroe–Rockall Plateau in relation to northeast Atlantic ridge-push and Alpine foreland stresses. *Tectonophysics*, *300*(1), 13–28. https://doi.org/10.1016/S0040-1951(98)00231-5

Bonnin, M., Nolet, G., Villaseñor, A., Gallart, J., & Thomas, C. (2014). Multiple-frequency tomography of the upper mantle beneath the African/Iberian collision zone. *Geophysical Journal International*, *198*(3), 1458–1473. https://doi.org/10.1093/gji/ggu214

Braun, J. (2006). Recent advances and current problems in modelling surface processes and their interaction with crustal deformation. *Geological Society, London, Special Publications*, *253*(1), 307–325. https://doi.org/10.1144/GSL.SP.2006.253.01.16

Brown, R. W., Beucher, R., Roper, S., Persano, C., Stuart, F., & Fitzgerald, P. (2013). Natural age dispersion arising from the analysis of broken crystals. Part I: Theoretical basis and implications for the apatite (U–Th)/He thermochronometer. *Geochimica et Cosmochimica Acta*, *122*, 478–497. https://doi.org/10.1016/j.gca.2013.05.041

Brun, M. V. L., & Lucazeau, F. (1988). Subsidence, extension and thermal history of the West African margin in Senegal. *Earth and Planetary Science Letters*, *90*(2), 204–220. https://doi.org/10.1016/0012-821X(88)90101-X

Burov, E., & Cloetingh, S. (1997). Erosion and rift dynamics: New thermomechanical aspects of post-rift evolution of extensional basins. *Earth and Planetary Science Letters*, *150*(1-2), 7–26. https://doi.org/10.1016/S0012-821X(97)00069-1

Burtner, R. L., Nigrini, A., & Donelick, R. A. (1994). Thermochronology of lower Cretaceous source rocks in the Idaho-Wyoming thrust belt. *AAPG Bulletin*, *78*(10), 1613–1636.

Charton, R., Bertotti, G., Arantegui, A., & Bulot, L. (2018). The Sidi Ifni transect across the rifted margin of Morocco (Central Atlantic): Vertical movements constrained by low-temperature thermochronology. *Journal of African Earth Sciences*, *141*, 22–32. https://doi.org/10.1016/j.jafrearsci.2018.01.006

Cloetingh, S., & Kooi, H. (1992). Intraplate stresses and dynamical aspects of rifted basins. *Tectonophysics*, *215*(1-2), 167–185. https://doi.org/10.1016/0040-1951(92)90080-P

Cogné, N., Gallagher, K., & Cobbold, P. R. (2011). Post-rift reactivation of the onshore margin of southeast Brazil: Evidence from apatite (U–Th)/He and fission-track data. *Earth and Planetary Science Letters*, *309*(1), 118–130. https://doi.org/10.1016/j.epsl.2011.06.025

Davison, I. (2005). Central Atlantic margin basins of North West Africa: Geology and hydrocarbon potential (Morocco to Guinea). *Journal of African Earth Sciences*, *43*(1-3), 254–274. https://doi.org/10.1016/j.jafrearsci.2005.07.018

Donelick, R. A., Ketcham, R. A., & Carlson, W. D. (1999). Variability of apatite fission-track annealing kinetics: II. Crystallographic orientation effects. *American Mineralogist*, *84*, 1224–1234.

Donelick, R. A., O'Sullivan, P. B., & Ketcham, R. A. (2005). Apatite fission-track analysis. *Reviews in Mineralogy and Geochemistry*, *58*(1), 49–94. https://doi.org/10.2138/rmg.2005.58.3

Dumitru, T. A. (1993). A new computer-automated microscope stage system for fission-track analysis. *Nuclear Tracks and Radiation Measurements*, *21*(4), 575–580. https://doi.org/10.1016/1359-0189(93)90198-I

Dunkl, I. (2002). Trackkey: A Windows program for calculation and graphical presentation of fission track data. *Computers & Geosciences*, *28*(1), 3–12. https://doi.org/10.1016/S0098-3004(01)00024-3

Eagles, G., & Wibisono, A. D. (2013). Ridge push, mantle plumes and the speed of the Indian plate. *Geophysical Journal International*, *194*(2), 670–677. https://doi.org/10.1093/gji/ggt162

Ehlers, T. A. (2005). Crustal thermal processes and the interpretation of thermochronometer data. *Reviews in Mineralogy and Geochemistry*, *58*(1), 315–350. https://doi.org/10.2138/rmg.2005.58.12

Ellouz, N., Patriat, M., Gaulier, J.-M., Bouatmani, R., & Sabounji, S. (2003). From rifting to Alpine inversion: Mesozoic and Cenozoic subsidence history of some Moroccan basins. *Sedimentary Geology*, *156*(1-4), 185–212. https://doi.org/10.1016/S0037-0738(02)00288-9

Ennih, N., & Liégeois, J.-P. (2008). The boundaries of the West African craton, with special reference to the basement of the Moroccan metacratonic Anti-Atlas belt. *Geological Society, London, Special Publications*, *297*(1), 1–17. https://doi.org/10.1144/SP297.1

Farley, K. A. (2002). (U-Th)/He dating: Techniques, calibrations, and applications. *Reviews in Mineralogy and Geochemistry*, *47*(1), 819–844. https://doi.org/10.2138/rmg.2002.47.18

Farley, K. A., Wolf, R. A., & Silver, L. T. (1996). The effects of long alpha-stopping distances on (U-Th)/He ages. *Geochimica et Cosmochimica Acta*, *60*(21), 4223–4229. https://doi.org/10.1016/S0016-7037(96)00193-7

Fitzgerald, P. G., Baldwin, S. L., Webb, L. E., & O'Sullivan, P. B. (2006). Interpretation of (U–Th)/He single grain ages from slowly cooled crustal terranes: A case study from the Transantarctic Mountains of southern Victoria Land. *Chemical Geology*, *225*(1–2), 91–120. https://doi.org/10.1016/j.chemgeo.2005.09.001

Flowers, R. M. (2009). Exploiting radiation damage control on apatite (U-Th)/He dates in cratonic regions. *Earth and Planetary Science Letters*, *277*(1-2), 148–155. https://doi.org/10.1016/j.epsl.2008.10.005

Flowers, R. M., Ketcham, R. A., Shuster, D. L., & Farley, K. A. (2009). Apatite (U–Th)/He thermochronometry using a radiation damage accumulation and annealing model. *Geochimica et Cosmochimica Acta*, *73*(8), 2347–2365. https://doi.org/10.1016/j.gca.2009.01.015

Frizon De Lamotte, D., Bezar, B. S., Bracène, R., & Mercier, E. (2000). The two main steps of the Atlas building and geodynamics of the western Mediterranean. *Tectonics*, *19*(4), 740–761. https://doi.org/10.1029/2000TC900003

Frizon De Lamotte, D., Leturmy, P., Missenard, Y., Khomsi, S., Ruiz, G., Saddiqi, O., et al. (2009). Mesozoic and Cenozoic vertical movements in the Atlas system (Algeria, Morocco, Tunisia): An overview. *Tectonophysics*, *475*(1), 9–28. https://doi.org/10.1016/j.tecto.2008.10.024

Gallagher, K. (2012). Transdimensional inverse thermal history modeling for quantitative thermochronology. *Journal of Geophysical Research*, *117*(B2), B02408. https://doi.org/10.1029/2011JB008825

Gallagher, K., & Brown, R. (1997). The onshore record of passive margin evolution. *Journal of the Geological Society*, *154*(3), 451–457. https://doi.org/10.1144/gsjgs.154.3.0451

Gallagher, K., Charvin, K., Nielsen, S., Sambridge, M., & Stephenson, J. (2009). Markov chain Monte Carlo (MCMC) sampling methods to determine optimal models, model resolution and model choice for Earth Science problems. *Marine and Petroleum Geology*, *26*(4), 525–535. https://doi.org/10.1016/j.marpetgeo.2009.01.003

Gallagher, K., & Ketcham, R. A. (2018). Comment on "Thermal history modelling: HeFTy vs. QTQt" by Vermeesch and Tian, Earth-Science Reviews (2014), 139, 279–290. *Earth-Science Reviews*, *176*, 387–394. https://doi.org/10.1016/j.earscirev.2017.11.001

Gautheron, C., Barbarand, J., Ketcham, R. A., Tassan-Got, L., van der Beek, P., Pagel, M., et al. (2013). Chemical influence on α-recoil damage annealing in apatite: Implications for (U–Th)/He dating. *Chemical Geology*, *351*, 257–267. https://doi.org/10.1016/j.chemgeo.2013.05.027

Gautheron, C., Tassan-Got, L., Ketcham, R. A., & Dobson, K. J. (2012). Accounting for long alpha-particle stopping distances in (U–Th–Sm)/He geochronology: 3D modeling of diffusion, zoning, implantation, and abrasion. *Geochimica et Cosmochimica Acta*, *96*, 44–56. https://doi.org/10.1016/j.gca.2012.08.016

Ghorbal, B., Bertotti, G., Foeken, J., & Andriessen, P. (2008). Unexpected Jurassic to Neogene vertical movements in 'stable' parts of NW Africa revealed by low temperature geochronology. *Terra Nova*, *20*(5), 355–363. https://doi.org/10.1111/j.1365-3121.2008.00828.x

Gleadow, A. J. W., Duddy, I. R., & Lovering, J. F. (1983). Fission track analysis: A new tool for the evaluation of thermal histories and hydrocarbon potential. *The APPEA Journal*, *23*(1), 93–102. https://doi.org/10.1071/aj82009

Gouiza, M. (2011). Mesozoic source-to-sink systems in NW Africa: Geology of vertical movements during the birth and growth of the Moroccan rifted margin, Ph. D Thesis, Vrije Universiteit Amsterdam, cloetingh, S.A.P.L. [Promotor]%%%%Hafid, M. [Promotor]%%%%Bertotti, G.V. [Copromotor].

Gouiza, M., Bertotti, G., & Andriessen, P. A. M. (2018). Mesozoic and Cenozoic thermal history of the Western Reguibat Shield (West African Craton). *Terra Nova*, *30*(2), 135–145. https://doi.org/10.1111/ter.12318

Gouiza, M., Bertotti, G., Hafid, M., & Cloetingh, S. (2010). Kinematic and thermal evolution of the Moroccan rifted continental margin: Doukkala-High Atlas transect. *Tectonics*, *29*, 22. https://doi.org/10.1029/2009TC002464

Gouiza, M., Charton, R., Bertotti, G., Andriessen, P., & Storms, J. E. A. (2017). Post-Variscan evolution of the Anti-Atlas belt of Morocco constrained from low-temperature geochronology. *International Journal of Earth Sciences*, *106*(2), 593–616. https://doi.org/10.1007/s00531-016-1325-0

Green, P. F., Duddy, I. R., Laslett, G. M., Hegarty, K. A., Gleadow, A. J. W., & Lovering, J. F. (1989). Thermal annealing of fission tracks in apatite 4. Quantitative modelling techniques and extension to geological timescales. *Chemical Geology: Isotope Geoscience*, *79*(2), 155–182. https://doi.org/10.1016/0168-9622(89)90018-3

Harman, R., Gallagher, K., Brown, R., Raza, A., & Bizzi, L. (1998). Accelerated denudation and tectonic/geomorphic reactivation of the cratons of northeastern Brazil during the Late Cretaceous. *Journal of Geophysical Research*, *103*(B11), 27,091–27,105. https://doi.org/10.1029/98JB02524

Hefferan, K. P., Admou, H., Karson, J. A., & Saquaque, A. (2000). Anti-Atlas (Morocco) role in Neoproterozoic Western Gondwana reconstruction. *Precambrian Research*, *103*(1–2), 89–96. https://doi.org/10.1016/S0301-9268(00)00078-4

Hoggard, M. J., Winterbourne, J., Czarnota, K., & White, N. (2017). Oceanic residual depth measurements, the plate cooling model, and global dynamic topography. *Journal of Geophysical Research: Solid Earth*, *122*(3), 2328–2372. https://doi.org/10.1002/2016JB013457

Japsen, P., Chalmers, J. A., Green, P. F., & Bonow, J. M. (2012). Elevated, passive continental margins: Not rift shoulders, but expressions of episodic, post-rift burial and exhumation. *Global and Planetary Change*, *90–91*, 73–86. https://doi.org/10.1016/j.gloplacha.2011.05.004

Ketcham, R. A., Carter, A., Donelick, R. A., Barbarand, J., & Hurford, A. J. (2007). Improved modeling of fission-track annealing in apatite. *American Mineralogist*, *92*(5-6), 799–810. https://doi.org/10.2138/am.2007.2281

Klitgord, K. D., Schouten, H., Vogt, P. R., & Tucholke, B. E. (1986). Plate kinematics of the central Atlantic. In *The Western North Atlantic Region: The Geology of North America* (pp. 351–378). USA: Geological Society of America.

Kneller, E. A., Johnson, C. A., Karner, G. D., Einhorn, J., & Queffelec, T. A. (2012). Inverse methods for modeling non-rigid plate kinematics: Application to mesozoic plate reconstructions of the Central Atlantic. *Computers & Geosciences*, *49*, 217–230. https://doi.org/10.1016/j.cageo.2012.06.019

Kusznir, N. J., & Park, R. G. (1987). The extensional strength of the continental lithosphere: Its dependence on geothermal gradient, and crustal composition and thickness. *Geological Society, London, Special Publications*, *28*(1), 35–52. https://doi.org/10.1144/GSL.SP.1987.028.01.04

Labails, C., Olivet, J.-L., Aslanian, D., & Roest, W. R. (2010). An alternative early opening scenario for the Central Atlantic Ocean. *Earth and Planetary Science Letters*, *297*(3-4), 355–368. https://doi.org/10.1016/j.epsl.2010.06.024

Le Roy, P. (1997). Les bassins ouest-marocains: Leur formation et leur évolution dans le cadre de l'ouverture et du développement de l'Atlantique central (marge africaine), Ph. D Thesis, Université de Bretagne Occidentale, France.

Le Roy, P., & Piqué, A. (2001). Triassic-Liassic Western Moroccan synrift basins in relation to the Central Atlantic opening. *Marine Geology*, *172*(3-4), 359–381. https://doi.org/10.1016/S0025-3227(00)00130-4

Leprêtre, R. (2015). Evolution phanérozoïque du Craton Ouest Africain et de ses bordures Nord et Ouest, Ph. D Thesis, Université Paris Sud - Paris XI.

Leprêtre, R., Barbarand, J., Missenard, Y., Gautheron, C., Pinna-Jamme, R., & Saddiqi, O. (2017). Mesozoic evolution of NW Africa: Implications for the Central Atlantic Ocean dynamics. *Journal of the Geological Society*, *174*(5), 817–835. https://doi.org/10.1144/jgs2016-100

Leprêtre, R., Barbarand, J., Missenard, Y., Leparmentier, F., & Frizon De Lamotte, D. (2014). Vertical movements along the northern border of the West African Craton: The Reguibat Shield and adjacent basins. *Geological Magazine*, *151*(05), 885–898. https://doi.org/10.1017/S0016756813000939

Leprêtre, R., Missenard, Y., Barbarand, J., Gautheron, C., Saddiqi, O., & Pinna-Jamme, R. (2015). Postrift history of the eastern central Atlantic passive margin: Insights from the Saharan region of South Morocco. *Journal of Geophysical Research: Solid Earth*, *120*(6), 4645–4666. https://doi.org/10.1002/2014JB011549

Li, Z. X., Bogdanova, S. V., Collins, A. S., Davidson, A., De Waele, B., Ernst, R. E., et al. (2008). Assembly, configuration, and break-up history of Rodinia: A synthesis. *Precambrian Research*, *160*(1), 179–210. https://doi.org/10.1016/j.precamres.2007.04.021

Lorencak, M., Kohn, B. P., Osadetz, K. G., & Gleadow, A. J. W. (2004). Combined apatite fission track and (U–Th)/He thermochronometry in a slowly cooled terrane: Results from a 3440-m-deep drill hole in the southern Canadian Shield. *Earth and Planetary Science Letters*, *227*(1), 87–104. https://doi.org/10.1016/j.epsl.2004.08.015

Malusà, M. G., Danišík, M., & Kuhlemann, J. (2016). Tracking the adriatic-slab travel beneath the tethyan margin of corsica–sardinia by low-temperature thermochronometry. *Gondwana Research*, *31*, 135–149. https://doi.org/10.1016/j.gr.2014.12.011

Mareschal, J. C., & Jaupart, C. (2004). Variations of surface heat flow and lithospheric thermal structure beneath the North American craton. *Earth and Planetary Science Letters*, *223*(1–2), 65–77. https://doi.org/10.1016/j.epsl.2004.04.002

Martínez-Loriente, S., Sallarès, V., Gràcia, E., Bartolome, R., Dañobeitia, J. J., & Zitellini, N. (2014). Seismic and gravity constraints on the nature of the basement in the Africa-Eurasia plate boundary: New insights for the geodynamic evolution of the SW Iberian margin. *Journal of Geophysical Research: Solid Earth*, *119*(1), 127–149. https://doi.org/10.1002/2013JB010476

Martín-Monge, A., Baudino, R., Gairifo-Ferreira, L. M., Tocco, R., Badalì, M., Ochoa, M., et al. (2017). An unusual Proterozoic petroleum play in Western Africa: The Atar Group carbonates (Taoudeni Basin, Mauritania), *Geological Society, London. Special Publications*, *438*(1), 119–157. https://doi.org/10.1144/SP438.5

McKenzie, D. (1978). Some remarks on the development of sedimentary basins. *Earth and Planetary Science Letters*, *40*(1), 25–32. https://doi.org/10.1016/0012-821X(78)90071-7

McKenzie, D., Jackson, J., & Priestley, K. (2005). Thermal structure of oceanic and continental lithosphere. *Earth and Planetary Science Letters*, *233*(3), 337–349. https://doi.org/10.1016/j.epsl.2005.02.005

Molnar, P. (2001). Climate change, flooding in arid environments, and erosion rates. *Geology*, *29*(12), 1071–1074. https://doi.org/10.1130/0091-7613(2001)029<1071:CCFIAE>2.0.CO;2

Müller, R. D., Seton, M., Zahirovic, S., Williams, S. E., Matthews, K. J., Wright, N. M., et al. (2016). Ocean basin evolution and global-scale plate reorganization events since Pangea breakup. *Annual Review of Earth and Planetary Sciences*, *44*(1), 107–138. https://doi.org/10.1146/annurev-earth-060115-012211

Ndiaye, M., Ngom, P. M., Gorin, G., Villeneuve, M., Sartori, M., & Medou, J. (2016). A new interpretation of the deep-part of Senegal-Mauritanian Basin in the Diourbel-Thies area by integrating seismic, magnetic, gravimetric and borehole data: Implication for petroleum exploration. *Journal of African Earth Sciences*, *121*, 330–341. https://doi.org/10.1016/j.jafrearsci.2016.06.002

O'Sullivan, P. B., & Parrish, R. R. (1995). The importance of apatite composition and single-grain ages when interpreting fission track data from plutonic rocks: A case study from the Coast Ranges, British Columbia. *Earth and Planetary Science Letters*, *132*(1–4), 213–224. https://doi.org/10.1016/0012-821X(95)00058-K

Piqué, A., & Laville, E. (1996). The central Atlantic rifting: Reactivation of Palaeozoic structures. *Journal of Geodynamics*, *21*(3), 235–255. https://doi.org/10.1016/0264-3707(95)00022-4

Purdy, G. M. (1987). Regional trends in the geology of the Appalachian-Caledonian-Hercynian-Mauritanide orogen. *Earth-Science Reviews*, *24*(4), 279–280. https://doi.org/10.1016/0012-8252(87)90063-8

Reiners, P. W., & Farley, K. A. (2001). Influence of crystal size on apatite (U–Th)/He thermochronology: An example from the Bighorn Mountains, Wyoming. *Earth and Planetary Science Letters*, *188*(3), 413–420. https://doi.org/10.1016/S0012-821X(01)00341-7

Rimi, A. (1990). Geothermal gradients and heat flow trends in Morocco. *Geothermics*, *19*(5), 443–454. https://doi.org/10.1016/0375-6505(90)90057-I

Rimi, A. (1999). Mantle heat flow and geotherms for the main geologic domains in Morocco. *International Journal of Earth Sciences*, *88*(3), 458–466. https://doi.org/10.1007/s005310050278

Rimi, A. (2000). Evidence of recent warming in the north of Morocco from disturbed geothermal gradients. *Geodinamica Acta*, *13*(1), 19–27. https://doi.org/10.1016/S0985-3111(00)00108-X

RodenTice, M. K., & Tice, S. J. (2005). Regional-scale mid-Jurassic to Late Cretaceous unroofing from the Adirondack Mountains through Central New England based on apatite fission-track and (UTh)/He thermochronology. *The Journal of Geology*, *113*(5), 535–552.

RodenTice, M. K., Tice, S. J., & Schofield, I. S. (2000). Evidence for differential unroofing in the Adirondack Mountains, New York State, determined by apatite fissiontrack thermochronology. *The Journal of Geology*, *108*(2), 155–169.

RodenTice, M. K., & Wintsch, R. P. (2002). Early Cretaceous normal faulting in Southern New England: Evidence from apatite and zircon fissiontrack ages. *The Journal of Geology*, *110*(2), 159–178.

Ruiz, G. M. H., Sebti, S., Negro, F., Saddiqi, O., Frizon de Lamotte, D., Stockli, D., et al. (2011). From central Atlantic continental rift to Neogene uplift–western Anti-Atlas (Morocco). *Terra Nova*, *23*(1), 35–41. https://doi.org/10.1111/j.1365-3121.2010.00980.x

Saddiqi, O., El Haimer, F.-Z., Michard, A., Barbarand, J., Ruiz, G., Mansour, E., et al. (2009). Apatite fission-track analyses on basement granites from south-western Meseta, Morocco: Paleogeographic implications and interpretation of AFT age discrepancies. *Tectonophysics*, *475*(1), 29–37. https://doi.org/10.1016/j.tecto.2009.01.007

Sahabi, M., Aslanian, D., & Olivet, J.-L. (2004). Un nouveau point de départ pour l'histoire de l'Atlantique central. *Comptes Rendus Geosciences*, *336*(12), 1041–1052. https://doi.org/10.1016/j.crte.2004.03.017

Schettino, A., & Turco, E. (2009). Breakup of Pangaea and plate kinematics of the central Atlantic and Atlas regions. *Geophysical Journal International*, *178*(2), 1078–1097. https://doi.org/10.1111/j.1365-246X.2009.04186.x

Schofield, D. I., Horstwood, M. S. A., Pitfield, P. E. J., Gillespie, M., Darbyshire, F., O'Connor, E. A., & Abdouloye, T. B. (2012). U–Pb dating and Sm–Nd isotopic analysis of granitic rocks from the Tiris Complex: New constaints on key events in the evolution of the Reguibat Shield, Mauritania. *Precambrian Research*, *204–205*, 1–11. https://doi.org/10.1016/j.precamres.2011.12.008

Sehrt, M., Glasmacher, U. A., Stockli, D. F., Jabour, H., & Kluth, O. (2017). Meso-/Cenozoic long-term landscape evolution at the southern Moroccan passive continental margin, Tarfaya Basin, recorded by low-temperature thermochronology. *Tectonophysics*, *717*, 499–518. https://doi.org/10.1016/j.tecto.2017.08.028

Sehrt, M., Glasmacher, U. A., Stockli, D. F., Jabour, H., & Kluth, O. (2018). The southern Moroccan passive continental margin: An example of differentiated long-term landscape evolution in Gondwana. *Gondwana Research*, *53*, 129–144. https://doi.org/10.1016/j.gr.2017.03.013

Sellwood, B. W., & Valdes, P. J. (2006). Mesozoic climates: General circulation models and the rock record. *Sedimentary Geology*, *190*(1), 269–287. https://doi.org/10.1016/j.sedgeo.2006.05.013

Shuster, D. L., Flowers, R. M., & Farley, K. A. (2006). The influence of natural radiation damage on helium diffusion kinetics in apatite. *Earth and Planetary Science Letters*, *249*(3–4), 148–161. https://doi.org/10.1016/j.epsl.2006.07.028

Soulaimani, A., Michard, A., Ouanaimi, H., Baidder, L., Raddi, Y., Saddiqi, O., & Rjimati, E. C. (2014). Late Ediacaran–Cambrian structures and their reactivation during the Variscan and Alpine cycles in the Anti-Atlas (Morocco). *Journal of African Earth Sciences*, *98*, 94–112. https://doi.org/10.1016/j.jafrearsci.2014.04.025

Spotila, J. A., G. C. Bank, Reiners, P. W., Naeser, C. W., Naeser, N. D., & Henika, B. S. (2004). Origin of the Blue Ridge escarpment along the passive margin of Eastern North America. *Basin Research*, *16*(1), 41–63. https://doi.org/10.1046/j.1365-2117.2003.00219.x

Steckler, M., & Watts, A. (1982). Subsidence history and tectonic evolution of Atlantic-type continental margins. *Dynamics of Passive Margins. AGU Geodyn. Ser*, *6*, 184–196.

Taylor, J. P., & Fitzgerald, P. G. (2011). Low-temperature thermal history and landscape development of the eastern Adirondack Mountains, New York: Constraints from apatite fission-track thermochronology and apatite (U-Th)/He dating. *GSA Bulletin*, *123*(3-4), 412–426. https://doi.org/10.1130/B30138.1

Teixell, A., Bertotti, G., Frizon de Lamotte, D., & Charroud, M. (2009). The geology of vertical movements of the lithosphere: An overview. *Tectonophysics*, *475*(1), 1–8. https://doi.org/10.1016/j.tecto.2009.08.018

Thiéblemont, D. (2016). Geological map of Africa at 1:10 million, doi:https://doi.org/10.14682/2016GEOAFR.

Torsvik, T. H., Rousse, S., Labails, C., & Smethurst, M. A. (2009). A new scheme for the opening of the South Atlantic Ocean and the dissection of an Aptian salt basin. *Geophysical Journal International*, *177*(3), 1315–1333. https://doi.org/10.1111/j.1365-246X.2009.04137.x

Tucholke, B. E., Sawyer, D. S., & Sibuet, J.-C. (2007). Breakup of the Newfoundland–Iberia rift. *Geological Society, London, Special Publications*, *282*(1), 9–46. https://doi.org/10.1144/SP282.2

Vermeesch, P., & Tian, Y. (2014). Thermal history modelling: HeFTy vs. QTQt. *Earth-Science Reviews*, *139*, 279–290. https://doi.org/10.1016/j.earscirev.2014.09.010

Villeneuve, M. (2005). Paleozoic basins in West Africa and the Mauritanide thrust belt. *Journal of African Earth Sciences*, *43*(1), 166–195. https://doi.org/10.1016/j.jafrearsci.2005.07.012

Villeneuve, M., & Cornée, J. (1994). Structure, evolution and palaeogeography of the West African craton and bordering belts during the Neoproterozoic. *Precambrian Research*, *69*(1-4), 307–326. https://doi.org/10.1016/0301-9268(94)90094-9

Watts, A. B. (1982). Tectonic subsidence, flexure and global changes of sea level. *Nature*, *297*(5866), 469–474. https://doi.org/10.1038/297469a0

Weber, U. D., Kohn, B. P., Gleadow, A. J. W., & Nelson, D. R. (2005). Low temperature Phanerozoic history of the Northern Yilgarn Craton, Western Australia. *Tectonophysics*, *400*(1), 127–151. https://doi.org/10.1016/j.tecto.2005.03.008

Ziegler, P. A., & Cloetingh, S. (2004). Dynamic processes controlling evolution of rifted basins. *Earth-Science Reviews*, *64*(1-2), 1–50. https://doi.org/10.1016/S0012-8252(03)00041-2